



## OPEN ACCESS

## EDITED BY

Javier Crespo,  
Marqués de Valdecilla Health Research  
Institute (IDIVAL), Spain

## REVIEWED BY

Joseph Barbi,  
University at Buffalo, United States  
Helena Solleiro-Villavicencio,  
Universidad Autónoma de la Ciudad de  
México, Mexico

## \*CORRESPONDENCE

Senad Divanovic  
✉ senad.divanovic@cchmc.org

## SPECIALTY SECTION

This article was submitted to  
Inflammation,  
a section of the journal  
Frontiers in Immunology

RECEIVED 15 November 2022

ACCEPTED 27 January 2023

PUBLISHED 17 February 2023

## CITATION

Oates JR, Sawada K, Giles DA, Alarcon PC,  
Damen MSMA, Szabo S, Stankiewicz TE,  
Moreno-Fernandez ME and Divanovic S  
(2023) Thermoneutral housing shapes  
hepatic inflammation and damage  
in mouse models of non-alcoholic  
fatty liver disease.  
*Front. Immunol.* 14:1095132.  
doi: 10.3389/fimmu.2023.1095132

## COPYRIGHT

© 2023 Oates, Sawada, Giles, Alarcon,  
Damen, Szabo, Stankiewicz,  
Moreno-Fernandez and Divanovic. This is an  
open-access article distributed under the  
terms of the [Creative Commons Attribution  
License \(CC BY\)](#). The use, distribution or  
reproduction in other forums is permitted,  
provided the original author(s) and the  
copyright owner(s) are credited and that  
the original publication in this journal is  
cited, in accordance with accepted  
academic practice. No use, distribution or  
reproduction is permitted which does not  
comply with these terms.

# Thermoneutral housing shapes hepatic inflammation and damage in mouse models of non-alcoholic fatty liver disease

Jarren R. Oates<sup>1,2,3</sup>, Keisuke Sawada<sup>1,2,3,4</sup>, Daniel A. Giles<sup>1,2,3</sup>,  
Pablo C. Alarcon<sup>1,2,3,4</sup>, Michelle S.M.A. Damen<sup>1,2</sup>, Sara Szabo<sup>1,5</sup>,  
Traci E. Stankiewicz<sup>1,2</sup>, Maria E. Moreno-Fernandez<sup>1,2</sup>  
and Senad Divanovic<sup>1,2,3,4,6\*</sup>

<sup>1</sup>Department of Pediatrics, University of Cincinnati College of Medicine, Cincinnati, OH, United States,

<sup>2</sup>Division of Immunobiology, Cincinnati Children's Hospital Medical Center, Cincinnati, OH, United States,

<sup>3</sup>Immunology Graduate Program, Cincinnati Children's Hospital Medical Center and the University of Cincinnati College of Medicine, Cincinnati, OH, United States, <sup>4</sup>Medical Scientist Training Program, University of Cincinnati College of Medicine, Cincinnati, OH, United States, <sup>5</sup>Division of Pathology, Cincinnati Children's Hospital Medical Center, Cincinnati, OH, United States, <sup>6</sup>Center for Inflammation and Tolerance, Cincinnati Children's Hospital Medical Center, Cincinnati, OH, United States

**Introduction:** Inflammation is a common unifying factor in experimental models of non-alcoholic fatty liver disease (NAFLD) progression. Recent evidence suggests that housing temperature-driven alterations in hepatic inflammation correlate with exacerbated hepatic steatosis, development of hepatic fibrosis, and hepatocellular damage in a model of high fat diet-driven NAFLD. However, the congruity of these findings across other, frequently employed, experimental mouse models of NAFLD has not been studied.

**Methods:** Here, we examine the impact of housing temperature on steatosis, hepatocellular damage, hepatic inflammation, and fibrosis in NASH diet, methionine and choline deficient diet, and western diet + carbon tetrachloride experimental models of NAFLD in C57BL/6 mice.

**Results:** We show that differences relevant to NAFLD pathology uncovered by thermoneutral housing include: (i) augmented NASH diet-driven hepatic immune cell accrual, exacerbated serum alanine transaminase levels and increased liver tissue damage as determined by NAFLD activity score; (ii) augmented methionine choline deficient diet-driven hepatic immune cell accrual and increased liver tissue damage as indicated by amplified hepatocellular ballooning, lobular inflammation, fibrosis and overall NAFLD activity score; and (iii) dampened western diet + carbon tetrachloride driven hepatic immune cell accrual and serum alanine aminotransferase levels but similar NAFLD activity score.

**Discussion:** Collectively, our findings demonstrate that thermoneutral housing has broad but divergent effects on hepatic immune cell inflammation and hepatocellular damage across existing experimental NAFLD models in mice. These insights may serve as a foundation for future mechanistic interrogations focused on immune cell function in shaping NAFLD progression.

## KEYWORDS

temperature, MCD, WD+CCl<sub>4</sub>, NAFLD, NASH, immune cells, inflammation

## Introduction

The unabated obesity pandemic (~1.5 billion people obese globally) is accompanied by a concomitant increase in the prevalence of non-alcoholic fatty liver disease (NAFLD). NAFLD, which affects approximately 25–30% of obese individuals, is considered the most common chronic liver disease and a leading cause for needing liver transplantation (1, 2). NAFLD encompasses a broad spectrum of liver conditions ranging from steatosis to non-alcoholic steatohepatitis (NASH) to cirrhosis, which eventually can progress to hepatocellular carcinoma (HCC) (1, 3). To study the broad aspects of NAFLD progression the field has traditionally employed a variety of experimental animal models. Notably, in mouse models of NAFLD, the strengths of each model are focused on select key parameters represented in human disease (e.g., steatosis, steatohepatitis, hepatocyte ballooning, Mallory-Denk bodies and fibrosis).

Prominent mouse models of NAFLD involve various dietary challenges including high fat diet (HFD), methionine choline deficient (MCD) diet, and chemical perturbations in combination with western diet (WD) (e.g., Carbon tetrachloride [CCl<sub>4</sub>] + WD diet) (3–6). HFD feeding drives robust obesity and hepatic recruitment of Kupffer cells and neutrophils, and only causes mild inflammation and minimal fibrosis (the latter only evident after prolonged HFD feeding) (7, 8). Conversely, MCD diet consistently induces robust hepatic immune cell recruitment, liver damage, and development of hepatic fibrosis, without the induction of obesity (9–11). Chemical perturbations, including high-dose CCl<sub>4</sub>, promote hepatic inflammation and fibrosis with induction of hepatocellular necrosis that is not consistent with human liver disease pathogenesis (9). As such, CCl<sub>4</sub> is used at lower doses and in combination with WD feeding to recapitulate histopathological manifestations of human NAFLD more accurately. However, unlike in human disease, this model is associated with weight loss (5). Nevertheless, despite being traditionally employed in studying NAFLD pathogenesis, the above discussed models only partly recapitulate clinical human disease progression. Notably, these shortcomings may limit the discovery of key cellular and molecular mechanisms underlying liver disease pathogenesis. Given that inflammation represents a unifying component of NAFLD progression (11–14) across the models used, further improvement of existing experimental models to enable discovery of mechanisms that shape inflammatory responses in NAFLD may represent the critical locus of the effect for translation of key discoveries to clinical relevance.

Ambient housing temperature regulates inflammatory responses to internal and external stimuli (15, 16). Common animal facilities house mice in thermo-stress (Ts) (20–23°C) conditions. Such

conditions however are associated with the activation of cold stress responses in mice, augmented production of stress hormone (e.g., corticosterone and catecholamine) which drives a multitude of physiological and metabolic changes (17, 18). Importantly, Ts housing suppresses immune responses including altered cellular energy availability, cytokine production, and lymphocyte egress from lymph nodes (15, 19–21). Conversely, thermoneutral (Tn) housing (29–34°C), a temperature where mice do not need to expend excess energy to maintain core body temperature, reverses the suppression of immune responsiveness observed at Ts housing conditions (1, 3, 16, 22). In the context of NAFLD, Tn housing coupled with HFD feeding accelerates and exacerbates disease progression and pathogenesis. Specifically, Tn housing in combination with HFD feeding enhances hepatic steatosis and inflammation, and hepatocellular damage in wild type C57BL/6 male mice and hepatic fibrosis in AKR mice (3). Further, wild type C57BL/6 female mice, which are generally resistant to HFD-induced obesity when housed at Ts conditions, developed robust obesity and NAFLD when housed at Tn conditions (3). Thus, the ability of Tn housing to reverse paradigms seen at Ts conditions by restricting immune suppression and promoting obesity in female mice warrants the examination of the impact of Tn housing on hepatic inflammation, steatosis, liver damage and development of hepatic fibrosis across multiple, traditionally used, experimental models of NAFLD in mice.

Here, we show that Tn housing shapes hepatic inflammation across multiple, traditionally used, experimental mouse models of NAFLD. In a model utilizing NASH diet, Tn housing augments obesity, serum ALT, hepatic immune cell accrual, expression of immune cell recruiting chemokines which correlates with increased lobular inflammation and liver disease as determined by NAFLD Activity Score (NAS). Similarly, in the MCD diet driven NAFLD model, Tn housing promotes increased hepatic expression of immune cell recruiting chemokines correlating with hepatic immune cell accrual, increased expression of fibrosis-associated genes and worsened fibrosis as indicated by increased cholangiolar proliferations accompanied by thicker collagenous pericellular fibers and overall increased NAS severity. Lastly, in the context of chemical perturbations combined with WD diet induced obesity, Tn housing decreases serum ALT which correlates with a decrease in hepatic immune cell accrual and modified immune cell inflammatory capacity. Collectively, these findings demonstrate for the very first time that thermoneutral housing has broad, yet divergent effects on hepatic immune cell inflammation and hepatocellular damage across existing experimental NAFLD models in C57BL/6 mice. As studies utilizing thermoneutral housing become more prevalent, insights gained may serve as a foundation for interrogation of mechanisms instructing immune cell function and development of future therapies to NAFLD.

## Materials and methods

### Mice and dietary studies

Wild type (WT) mouse breeding pairs, originally purchased from Jackson Laboratories, were on C57BL/6J background, housed at thermo-stress (Ts; 22°C) conditions with free access to autoclaved

**Abbreviations:** NAFLD, Non-alcoholic fatty liver disease; HFD, High fat diet; MCD, Methionine Choline Deficient; CCl<sub>4</sub>, Carbon tetrachloride; WD+CCl<sub>4</sub>, Western diet + CCl<sub>4</sub>; NASH, Non-alcoholic steatohepatitis; HCC, Hepatocellular carcinoma; Ts, Thermostress; Tn, Thermoneutrality; NAS, NAFLD activity score; ALT, Alanine transaminase; WD, Western diet; WAT, White adipose tissue; LD-MS, Large droplet macrovesicular steatosis; SD-MS, Small droplet macrovesicular steatosis; mRNA, Messenger Ribonucleic Acid; PMA, Phorbol 12-myristate 13-acetate; AST, Aspartate transaminase; H&E, Hematoxylin and Eosin.

food and water, and bred at Cincinnati Children's Hospital Medical Center (CCHMC) in a specific pathogen-free (spf) facility. Only 8-week-old WT male mice were used in our studies. For our studies, 6-week old mice were maintained at Ts or placed at thermoneutral (Tn; 30°C with 30% humidity) conditions for 2 weeks to allow acclimation prior to the initiation of dietary challenge. Tn housing was accomplished using Caron chambers (Caron Products & Services, INC). For all studies, food and water were replaced weekly. Body weight was recorded weekly. Corn cob bedding was used in the housing of all mice. All animal care was provided in accordance with the Guide for the Care and Use of Laboratory Animals. All studies were approved by the Cincinnati Children's Hospital Medical Center IACUC.

### **Chow diet**

WT C57BL/6 mice (8-week-old) were fed CD (fat 13.5% kcal, carbohydrate 59% kcal, protein 27.5% kcal; LabDiet 5010) and housed at either Ts or Tn as controls to specific dietary challenge experiments.

### **Methionine-choline deficient diet**

WT C57BL/6 mice (8-week-old) were fed MCD diet (MCD; Research Diets #A02082002B; 16% Protein, 63% Carbohydrate and 21% Fat kcal/gram) and housed at either Ts or Tn for 4 or 10 weeks as previously described (10, 23).

### **NASH diet**

WT C57BL/6 mice (8-week-old) were fed a NASH diet (40% kcal fat, 20% kcal fructose, and 2% kcal cholesterol by weight; Research diets, D09100301) and housed at either Ts or Tn for 22 weeks as previously described (24).

### **Carbon tetrachloride ( $\text{CCl}_4$ )**

WT C57BL/6 mice (8-week-old) were fed CD.  $\text{CCl}_4$  (Sigma-Aldrich, 289116-100ML) was injected with the dose of 2  $\mu\text{l}$  (0.32  $\mu\text{g}$ )/g of body weight, of  $\text{CCl}_4$  or olive oil (control) i.p. 2x weekly for 3 weeks.

### **Western diet + carbon tetrachloride (WD+ $\text{CCl}_4$ )**

WT C57BL/6 mice (8-week-old) were fed a WD (21.1% fat, 41% Sucrose, and 1.25% Cholesterol by weight; Teklad diets, TD. 120528) and a high sugar solution (23.1 g/L d-fructose and 18.9 g/L d-glucose) in drinking water.  $\text{CCl}_4$  (Sigma-Aldrich, 289116-100ML), 0.2  $\mu\text{l}$  (0.32  $\mu\text{g}$ )/g of body weight or corn oil (control) was i.p. injected once per week, as previously described (5, 24) for 12 weeks.

## **Hepatic immune cell isolation**

Hepatic immune cells were isolated using Miltenyi Biotec Gentlemax technology followed by Percoll gradient. Briefly, whole liver was homogenized using Miltenyi Gentlemax C tubes using RPMI + 10% fetal bovine serum. After resuspension, cells were centrifuged at 2000 rpm for 10 minutes. Cell pellets were homogenized in a 33% Percoll solution (Sigma-Aldrich) diluted in RPMI medium 1640 (Gibco). Following gradient separation, and

lysing of red blood cells, hepatic infiltrating immune cells were subsequently analyzed by flow cytometry (3, 25, 26).

## **Hepatic function**

Hepatic triglycerides (TGs) were quantified using Triglyceride Reagent and Triglyceride Standards (Pointe Scientific). Serum alanine aminotransferase (ALT) and aspartate aminotransferase levels (AST) were quantified using ALT Reagent, AST Reagent and Catalase I and II (Catachem). For histology, liver tissue was fixed in 10% buffered formalin, and stained with H&E or Masson's trichrome and evaluated by a board-certified pathologist (3, 24).

## **Hepatic immune cell characterization**

To determine immune cell population single cell suspensions derived from hepatic tissues, isolated immune cells were labeled with monoclonal antibodies. For cytokine production, total single cells were stimulated for 4 hours with Phorbol 12-myristate 13-acetate (PMA; 50 ng/ml) (Sigma-Aldrich, St. Louis, MO) and Ionomycin (1  $\mu\text{g}/\text{ml}$ ) (EMD Millipore), in presence of Brefeldin A (10  $\mu\text{g}/\text{mL}$ ) (GoldBio). Subsequently, data were collected using an LSR Fortessa (BD) and Cytek Aurora (Cytek Biosciences) and analyzed using FlowJo X software (vX10).

## **Immune cell characterization was as follows**

### **CD4 $^{+}$ T cells**

Mouse cells were stained with Live/Dead stain (Zombie UV Dye: Biolegend) and with directly-conjugated monoclonal antibodies to CD45-PE-Dazzle594 (Biolegend, 104), TCR $\beta$ -APCe780 or APC (Invitrogen, H57-597), CD4-APC-eF780 or BV786 (e-Biosciences, RM4-5), then fixed, permeabilized and stained for the cytokines IL-17A-PerCpCy5.5 or PE (e-Biosciences, 17B7), IFN $\gamma$ -PE-Cy7 (e-Biosciences, XMG1.2) and TNF $\alpha$ -BV650 (Biolegend, MP6-XT22).

### **CD8 $^{+}$ T cells**

Mouse cells were stained with Live/Dead stain (Zombie UV Dye: Biolegend) and with directly-conjugated monoclonal antibodies to CD45-PE-Dazzle594 (Biolegend, 104), TCR $\beta$ -APCe780 or APC (Invitrogen, H57-597), CD8-BV510 (Biolegend, 53-6.7), then fixed, permeabilized and stained for the cytokines IL-17A-PerCpCy5.5 or PE (e-Biosciences, 17B7), IFN $\gamma$ -PE-Cy7 (e-Biosciences, XMG1.2) and TNF $\alpha$ -BV650 (Biolegend, MP6-XT22).

### **Macrophages**

Mouse cells were stained with Live/Dead stain (Zombie UV Dye: Biolegend) and with directly conjugated monoclonal antibodies to CD45-PE-Dazzle594 (Biolegend, 104), CD11b-eF450 (Biolegend, 17A2), F4/80-APC (eBiosciences, BM8) then fixed, permeabilized and stained for the cytokine TNF $\alpha$ -BV650 (Biolegend, MP6-XT22).

## NK cells

Mouse cells were stained with Live/Dead stain (Zombie UV Dye: Biolegend) and with directly conjugated monoclonal antibodies to CD45-PE-Dazzle594 (Biolegend, 104), NK1.1-BV711 (Biolegend, PK136) then fixed, permeabilized and stained for the cytokine IFN $\gamma$ -PE-Cy7 (e-Biosciences, XMG1.2).

## NKT cells

Mouse cells were stained with Live/Dead stain (Zombie UV Dye: Biolegend) and with directly conjugated monoclonal antibodies to CD45-PE-Dazzle594 (Biolegend, 104), NK1.1-BV711 (Biolegend, PK136) and TCR $\beta$ -APCe780 or APC (Invitrogen, H57-597).

## B cells

Mouse cells were stained with Live/Dead stain (Zombie UV Dye: Biolegend) and with directly conjugated monoclonal antibodies to CD45-PE-Dazzle594 (Biolegend, 104) and B220-BV605 (Biolegend, RA3-6B2).

## Neutrophils

Mouse cells were stained with Live/Dead stain (Zombie UV Dye: Biolegend) and with directly conjugated monoclonal antibodies to CD45-PE-Dazzle594 (Biolegend, 104), CD11b-eF450 (Biolegend, 17A2), Gr1-FITC (Invitrogen, RB6-8C5) then fixed, permeabilized and stained for the cytokine TNF $\alpha$ -BV650 (Biolegend, MP6-XT22).

## mRNA and qPCR analysis

Tissue samples were homogenized in TRIzol. RNA was extracted, reverse transcribed to complementary DNA (cDNA), and subjected

to qPCR analysis (Light Cycler 480 II; Roche Diagnostics) as previously described (3, 15). The primer sequences, all from Invitrogen are as follows see below:

## Statistical analysis

For statistical analysis, normality and lognormality tests and parametric tests were employed as determined by the Graphpad Prism software. A 2-tailed student's *t* test was used when the comparison was between 2 groups, while a 1-way ANOVA with Tukey's *post hoc* test to assess differences between specific groups was employed for 3 or more groups. Statistical analysis was completed using Prism 5a (GraphPad Software Inc.). All values are represented as means  $\pm$  SEM. A *P*-value less than 0.05 was considered significant.

## Results

### Tn housing augments NASH diet driven myeloid immune cell accrual in the liver and exacerbates liver disease pathogenesis

Our initial investigation focused on determining the impact of Tn housing on liver damage at homeostatic conditions. Tn housing did not impact body weight and promoted a slight reduction in wet liver weights, compared to Ts. Importantly, both Tn and Ts housed animals displayed similar serum ALT levels (Supplementary Figures 1A–C). As coupling high fat diet (HFD)-driven obesity with Tn housing exacerbates

Primer	Forward Sequence 5'-3'	Reverse Sequence 5'-3'
Ccl2	AGATGCAGTTAACGCCAAC	TGTCTGGACCCATTCCCTCTTG
Ccl3	ACCATGACACTCTGCAACCAAG	TTGGAGTCAGCGCAGATCTG
Tnfa	CCAGACCCCTCACACTCAGATCA	CACTTGGTGGTTGCTACGAC
Ifng	TGGCTGTTCTGGCTGTTACTG	ACGCTTATGTTGCTGATG
Il6	TGGTACTCCAGAAGACCAGAGG	AACGATGATGCACCTGCAGA
Ki67	ATCAATTGACCGCTCCTTAGGT	GCTCGCTTGATGGTTCCCT
Ccnd1	GCGTACCCCTGACACCAATCTC	CTCCTTTCGCACCTCTGCTC
Col1a1	GGTTTCCACGTCTCACCATT	ACATGTTCAGCTTGTGGACC
Col1a2	AGCAGGTCTTGAAACCTT	AAGGAGTTTCATCTGGCCCT
Acta2	GTTCAGTGGTGCCTCTGTCA	GGGATCCTGACGCTGAAGTA
H19	CAACATCCCACCCACCGTAA	GCTCACCAAGAAGGCTGGAT
Afp	TCTTTCCACTCCACTTGGC	GGCGATGGGTGTTAGAAAG
ChrebP	TCTGCAGATCGCGTGGAG	CTTGTCCCGGCATAGCAAC
Srebp	CTGTCTCACCCCCAGCATAG	GATGTGCGAAGTGGACACAG
Lxra	CTCAATGCCTGATGTTCTCCT	TCCAACCTATCCCTAAAGCAA
Lipe	TCTCGTTGCCTTGAGTGC	ACGCTACACAAAGGCTGCTT
Pparg	GAATGCGAGTGGCTTCCAT	TGCACTGCCTATGAGCACTT
Irs1	CTCCGTCTAACATCCACCTTG	AGCTCGCTAACTGAGATGTCAT
B actin	GGCCCAGAGCAAGAGAGGTA	GGTTGGCCTTAGGTTTCAGG

inflammatory responsiveness and accelerates NAFLD pathogenesis (3), we next examined the impact of Tn housing in a model of obesogenic diet-driven NAFLD, a diet rich in cholesterol and sugars that has been postulated to mimic human disease (27–29). To mimic these conditions, Ts and Tn housed C57BL/6 wild type male mice were fed a NASH diet for 22 weeks (Figure 1A). Tn housed mice, compared to Ts housed counterparts, had increased total body weight gain over time ( $p=0.01$ ) (Figure 1B). Further examination of visceral white adipose tissue (WAT) depots revealed that Tn housing dominantly impacted perirenal WAT fat redistribution ( $p=0.04$ ) rather than inguinal and epididymal WAT depots (Supplementary Figure 2A).

Given the observed changes in obesity and adiposity in Tn housed mice, we analyzed the impact of Tn housing on gross liver histology. Obesity is associated with ectopic fat deposition in the liver, thus the impact of Tn housing on NASH diet-driven hepatic steatosis and hepatocellular damage was examined. Both Tn and Ts housed, NASH diet fed mice displayed equal presence of classic large droplet macrovesicular steatosis (LD-MS; a single large steatotic droplet replaces nearly the entire cytoplasm and pushes the nucleus peripherally) and small droplet macrovesicular steatosis (SD-MS; numerous smaller droplets of fat that replace essentially the entire cytoplasm and expand the cell) (Figures 1C, D) (see arrows). Congruently, both Tn and Ts housed, NASH diet fed mice had similar

wet liver weights (Supplementary Figure 2B) and hepatic triglyceride accumulation (Supplementary Figure 2C). However, additional histological examination revealed that despite similar hepatocyte ballooning, Tn housed NASH-diet-fed mice, compared to Ts housed counterparts, exhibited increased focal lobular inflammation ( $p=0.05$ ), and had an overall increase in NAFLD Activity Score (NAS) severity ( $p=0.04$ ) (Figures 1C, depicted in E) (see arrows). Lastly, in agreement with histological analyses, the Tn housed, NASH diet fed mice, compared to Ts housed counterparts, had exacerbated serum alanine transaminase (ALT) levels ( $p=0.01$ ) (Figure 1F).

Hepatocellular damage is closely linked with altered hepatic inflammation. Hence, we next examined the impact of Tn housing on NASH diet-driven hepatic inflammation, hepatic immune cell composition and immune cell inflammatory capacity. Tn and Ts housed, NASH diet fed mice had similar hepatic mRNA expression of *Tnfa*, a proinflammatory cytokine that contributes to hepatic inflammation and damage (30, 31) (Supplementary Figure 2D). However, Tn housing increased hepatic mRNA expression of immune cell recruiting chemokines *Ccl2* ( $p=0.000009$ ) and *Ccl3* ( $p=0.04$ ) (Supplementary Figure 2E). Subsequent analysis of the immune cell composition demonstrated that Tn housing promoted an increase in total hepatic immune cell accrual ( $p=0.04$ ) in context of NASH diet feeding (Supplementary Figure 2F). Cellular characterization of hepatic

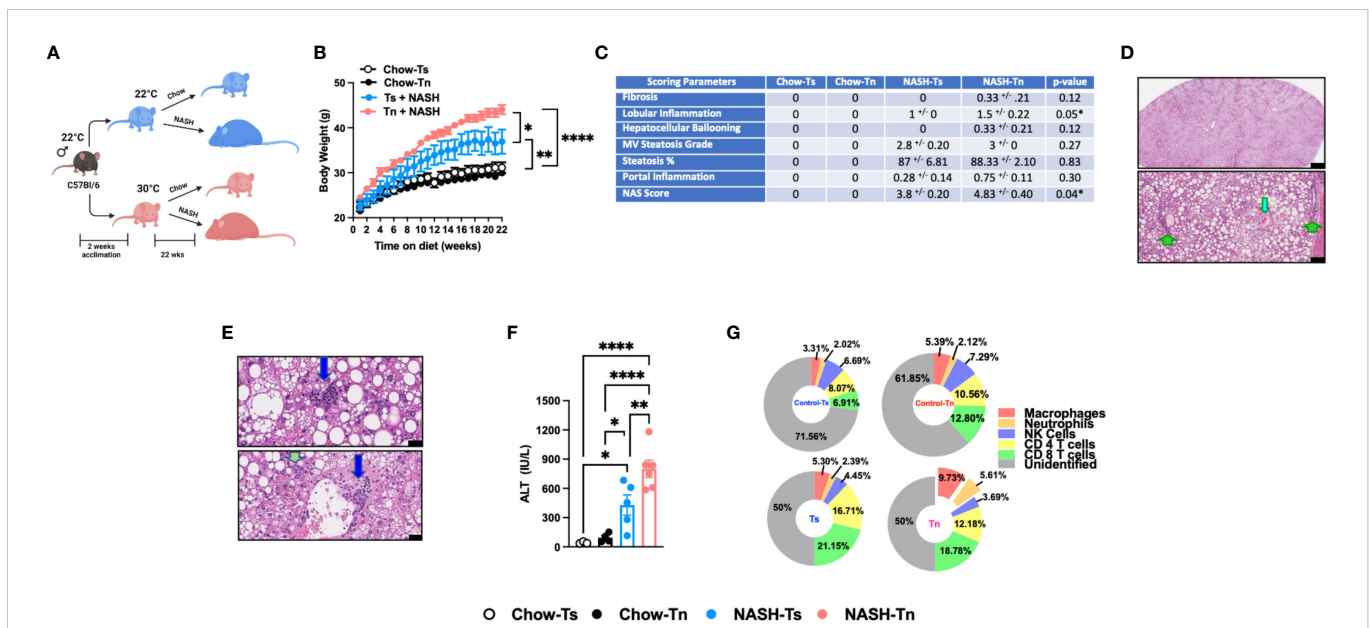


FIGURE 1

Tn housing augments NASH diet driven myeloid immune cell accrual in the liver and exacerbates liver disease pathogenesis. (A) Schematic of the experimental design. Eight-week-old WT mice maintained at Ts or acclimated to Tn for 2 weeks prior to study initiation were fed a chow (baseline reference) or NASH diet for 22 weeks. During the course of 22 weeks, (B) body weights of Ts and Tn housed mice were recorded. At the conclusion of the study, additional parameters of NAFLD severity were analyzed. (C) The liver tissue was preserved in formalin, stained with hematoxylin and eosin (H&E), and analyzed by a clinical pathologist. Table depicting histological scoring analyses for fibrosis, lobular inflammation, hepatocellular ballooning, macrovesicular (MV) steatosis grade, steatosis percentage, portal inflammation and NAFLD activity score (NAS) severity. (D) (Top) Extensive steatosis (80-95%) on H&E with a combination of classic large droplet macrovesicular steatosis (LD-MS) and small droplet (SD-MS) macrovesicular steatosis. Portae: green arrows. Central veins: light blue arrows. (Bottom) Black bar = 629 $\mu$ m; (Middle) Black bar = 109 $\mu$ m. (E) Liver H&E staining. (Top) Ballooning (yellow arrow). (Middle) Focal portal inflammation, perivenular (blue arrow), with small focus of cholangiolar reactivity (green arrow). Black bar = 25 $\mu$ m. (Bottom) Example for focal lobular inflammation (lymphocytic) (blue arrow), classic for NAFLD. Black bar = 33 $\mu$ m. (F) Hepatocellular damage as quantified by serum ALT levels collected at the conclusion of the study. (G) Hepatic inflammation as defined by flow cytometric analyses of hepatic immune cell accrual at the conclusion of the study. Donut charts depicting liver immune compositions (macrophages, neutrophils, CD4<sup>+</sup> cells, CD8<sup>+</sup> cells, NK cells, and unidentified cells) as determined by flow cytometry from percent of CD45<sup>+</sup> population. In bar graphs, data represent mean +/- SEM. (B, C, F, G) Representative of 2 individual experiments (n=5-6/condition). (F) One-way ANOVA. \*P<0.05, \*\* P<0.01, \*\*\*\* P<0.0001.

immune infiltrate in Tn housed NASH-diet-fed mice, compared to Ts housed counterparts, revealed specific increase in frequencies and absolute numbers of macrophages ( $CD45^+CD11b^+F4/80^+$ ) ( $p=0.03$ ) and neutrophils ( $CD45^+CD11b^+Gr1^+$ ) ( $p=0.03$ ), but reduced frequency of  $CD4^+$  T cells ( $CD45^+CD3^+CD4^+$ ) (Figure 1G and Supplementary Table 1, for gating strategy see Supplementary Figure 3). However, despite the apparent changes in hepatic immune cell composition, the inflammatory capacity of hepatic immune cells following PMA/ionomycin stimulation (Supplementary Figures 2G, H) was similar in Tn and Ts housed, NASH diet fed mice.

Prolonged hepatic inflammation induces tissue damage and development of hepatic fibrosis (32, 33). However, traditional HFD feeding does not induce robust hepatic fibrosis in C57BL/6 wild type mice under Ts housing conditions. Notably, diets high in cholesterol and sugar (i.e., fructose and sucrose) content are known to yield upregulation of pathways associated with fibrosis and promote histological patterns of fibrosis that mimic fibrosis-like characteristics seen in human disease (34, 35). Hence, the impact of Tn housing on hepatic fibrosis was examined. Tn and Ts housed NASH-diet-fed mice had similar expression of fibrosis associated genes *Col1a1*, *Col1a2* and *Acta2* in the liver (Supplementary Figure 2I). Congruently, both Tn and Ts housed, NASH diet fed mice had minimal fibrosis in association with periportal cholangiolar reactivity as determined by trichrome staining (Figure 1C and Supplementary Figure 2J).

NAFLD is also associated with dysregulated lipid metabolism and insulin signaling, both of which contribute to development and severity of metabolic syndrome (36, 37). Obesity in particular is associated with dysregulation of lipid metabolism and insulin signaling pathways (36, 37). Hence, the impact of Tn housing on pathways associated with lipid metabolism and insulin signaling were next examined. Notably, Tn and Ts housed, NASH diet fed mice, despite differences in NAFLD severity, had similar hepatic expression of insulin signaling (*Pparγ* and *Irs1*) and lipid metabolism-associated genes (*Lxra*, *Lipe*, *Chreb1*, and *Srebp*) (Supplementary Figures 2K–L).

## Tn housing augments MCD diet driven myeloid immune cell accrual in the liver and exacerbates liver disease pathogenesis

Increased incidence of NAFLD is reported to also occur in the absence of obesity (38). Using the MCD diet model of NAFLD, which induces weight loss but promotes hepatic steatosis, inflammation, and hepatocellular damage, we next examined whether Tn housing enhanced NAFLD pathogenesis in an obesity independent setting. Tn and Ts housed C57BL/6 wild type male mice were fed MCD diet for 4 weeks (Figure 2A). Tn housing did not impact MCD diet driven weight loss – a key characteristic of MCD diet feeding (Figure 2B). Hepatic triglycerides levels were similar despite increased liver to body weight ratio ( $p=0.005$ ) in Tn housed, MCD diet fed mice (Supplementary Figures 4A, B). However, histopathological analyses revealed that Tn housed, MCD diet fed mice, compared to Ts housed counterparts, exhibited a higher macrovesicular steatosis grade ( $p=0.04$ ) (Figures 2C, D, see green arrows). In addition, Tn housed, MCD diet fed mice, compared to Ts housed counterparts, had increased overall hepatocellular damage as evidenced by increased

focal inflammation ( $p=0.003$ ) and necrosis (acidophil bodies) (Figure 2E, see red arrows), and a significant increase in NAS severity ( $p=0.004$ ) (Figure 2C), but had similar ALT and Aspartate aminotransferase (AST) levels (Figure 2F and Supplementary Figure 4C). Tn housed, MCD diet fed mice, compared to Ts counterparts, exhibited comparable hepatic expression levels of *Tnfa*, *Ccl2* and *Ccl3* in total liver tissue (Supplementary Figures 4D, E). Similarly, analysis of the immune cell composition showed comparable numbers of total hepatic immune cells (Supplementary Figure 4F). Characterization of hepatic immune cell infiltrate revealed that Tn housing in combination with MCD diet feeding promoted a specific increase in frequencies and absolute numbers of macrophages (frequency  $p=0.01$ ; absolute #  $p=0.01$ ) and neutrophils (frequency  $p=0.0002$ ; absolute #  $p=0.001$ ) and a decrease in  $CD4^+$  and  $CD8^+$  T cells absolute numbers (Figure 2G and Supplementary Table 2). Nevertheless, despite the changes in hepatic immune cell composition, the inflammatory capacity of these cells following *ex vivo* PMA/ionomycin stimulation was not altered (Supplementary Figures 4G, H).

MCD diet is a well-accepted experimental model of hepatic fibrosis (9, 39, 40). Whether Tn housing modifies development of hepatic fibrosis in the context of MCD feeding is unknown. Tn and Ts housed, MCD diet fed mice exhibited similar hepatic expression of fibrosis associated genes *Col1a1*, *Col1a2* and *Acta2* ( $p=0.18$ ) (Supplementary Figure 4I). Nevertheless, Tn housed, MCD diet fed mice, compared to Ts housed counterparts, had worsened hepatic fibrosis as indicated by increased cholangiolar proliferations accompanied by thicker collagenous pericellular fibers (Figures 2C, H, see green arrows). MCD diet does not induce metabolic syndrome (9, 41). We next examined whether Tn housing would be sufficient to alter the expression of lipid metabolism- and insulin signaling-associated genes linked with metabolic syndrome in NAFLD (36, 37). Notably, Tn and Ts housed, MCD diet fed mice, despite differences in NAFLD severity, exhibited similar hepatic expression of insulin signaling (*Pparγ* and *Irs1*) and lipid metabolism-associated genes (*Lxra*, *Lipe*, *Chreb1*, and *Srebp*) (Supplementary Figures 4J, K).

Prolonged MCD feeding exacerbates NASH pathology (10). To further define the impact of Tn housing on prolonged MCD-driven NAFLD, C57BL/6 wild type mice were housed at Tn and Ts and fed MCD diet for 10 weeks (Supplementary Figure 5A). Similar to 4 weeks of MCD diet feeding, no differences in weight loss over time between Tn and Ts housed mice were observed (Supplementary Figure 5B). Tn housed, MCD diet fed mice, compared to Ts counterparts, had decreased liver to body weight ratio ( $p=0.003$ ) and similar total hepatic triglyceride accumulation compared to Ts housed counterparts (Supplementary Figures 5C, D), but displayed exacerbated steatosis percentage ( $p=0.03$ ) (detected in 85–95% range) (Supplementary Figure 5E). Additional histological examination revealed that Tn housed, MCD diet fed mice, compared to Ts housed counterparts, had increased hepatocellular ballooning ( $p=0.01$ ), multifocal lobular inflammation ( $p=0.01$ ), and the overall NAS severity ( $p=0.005$ ) (Supplementary Figure 5E), yet ALT and AST remained similar (Supplementary Figures 5F, G). Further, extended MCD diet feeding in Tn housed mice resulted in significantly increased hepatic expression of *Tnfa* ( $p=0.004$ ), *Ccl2* ( $p=0.02$ ) and *Ccl3* ( $p=0.01$ ) (Supplementary Figures 5H–I). Despite similar absolute numbers of total hepatic immune cells (Supplementary Figure 5J), Tn

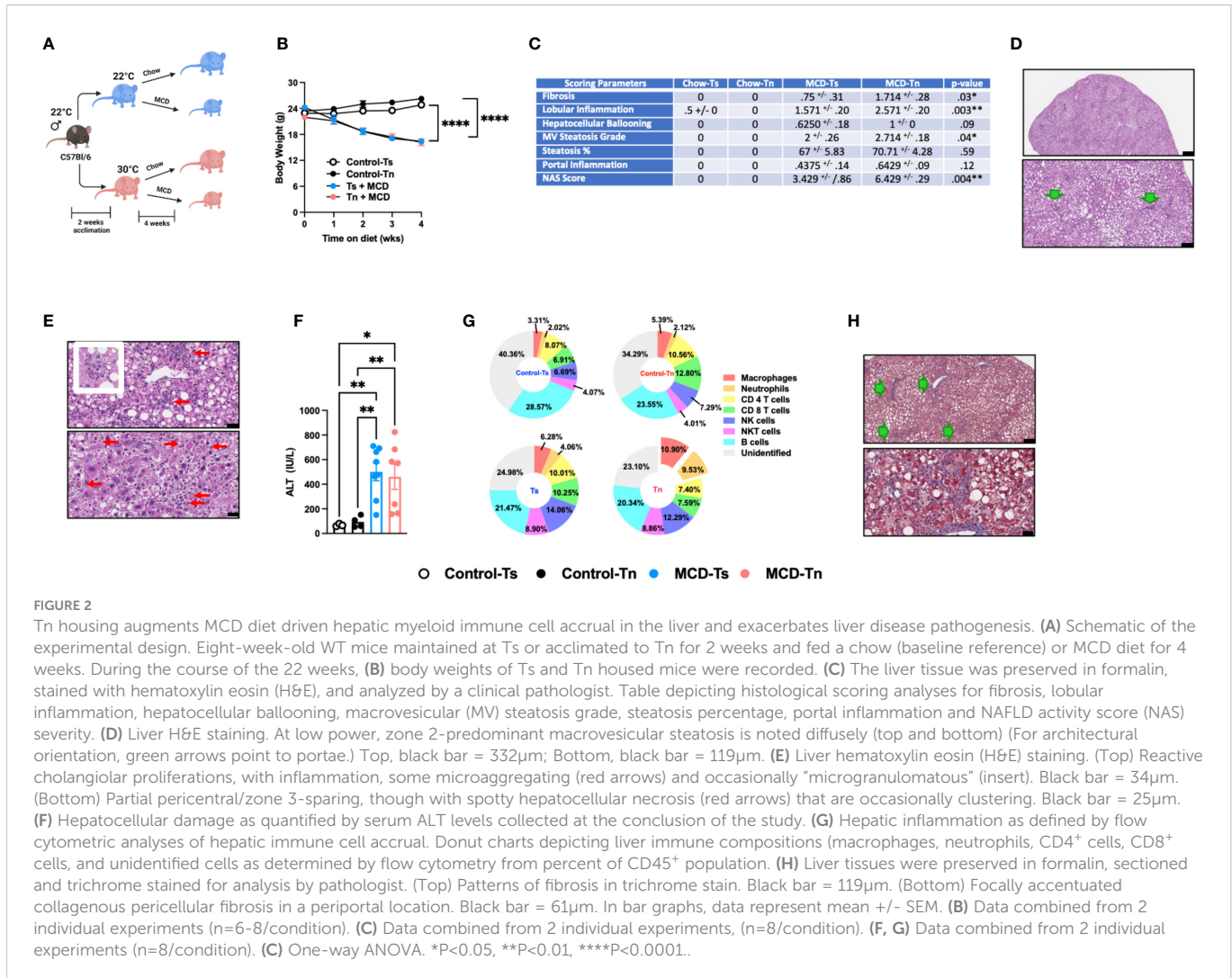


FIGURE 2

Tn housing augments MCD diet driven hepatic myeloid immune cell accrual in the liver and exacerbates liver disease pathogenesis. (A) Schematic of the experimental design. Eight-week-old WT mice maintained at Ts or acclimated to Tn for 2 weeks and fed a chow (baseline reference) or MCD diet for 4 weeks. During the course of the 22 weeks, (B) body weights of Ts and Tn housed mice were recorded. (C) The liver tissue was preserved in formalin, stained with hematoxylin/eosin (H&E), and analyzed by a clinical pathologist. Table depicting histological scoring analyses for fibrosis, lobular inflammation, hepatocellular ballooning, macrovesicular (MV) steatosis grade, steatosis percentage, portal inflammation and NAFLD activity score (NAS) severity. (D) Liver H&E staining. At low power, zone 2-predominant macrovesicular steatosis is noted diffusely (top and bottom) (For architectural orientation, green arrows point to portae.) Top, black bar = 332 $\mu$ m; Bottom, black bar = 119 $\mu$ m. (E) Liver hematoxylin/eosin (H&E) staining. (Top) Reactive cholangiolar proliferations, with inflammation, some microaggregating (red arrows) and occasionally "microgranulomatous" (insert). Black bar = 34 $\mu$ m. (Bottom) Partial pericentral/zone 3-sparing, though with spotty hepatocellular necrosis (red arrows) that are occasionally clustering. Black bar = 25 $\mu$ m. (F) Hepatocellular damage as quantified by serum ALT levels collected at the conclusion of the study. (G) Hepatic inflammation as defined by flow cytometric analyses of hepatic immune cell accrual. Donut charts depicting liver immune compositions (macrophages, neutrophils, CD4 $^{+}$  cells, CD8 $^{+}$  cells, and unidentified cells as determined by flow cytometry from percent of CD45 $^{+}$  population. (H) Liver tissues were preserved in formalin, sectioned and trichrome stained for analysis by pathologist. (Top) Patterns of fibrosis in trichrome stain. Black bar = 119 $\mu$ m. (Bottom) Focally accentuated collagenous pericellular fibrosis in a periportal location. Black bar = 61 $\mu$ m. In bar graphs, data represent mean +/- SEM. (B) Data combined from 2 individual experiments (n=6-8/condition). (C) Data combined from 2 individual experiments (n=8/condition). (F, G) Data combined from 2 individual experiments (n=8/condition). (C) One-way ANOVA. \*P<0.05, \*\*P<0.01, \*\*\*\*P<0.0001.

housed, MCD diet fed mice, compared to Ts housed counterparts, had a significant increase in hepatic frequency of macrophage ( $p=0.001$ ) and neutrophil ( $p=0.01$ ) accrual (Supplementary Figure 5K). Surprisingly, hepatic macrophages isolated from these mice had uniquely blunted inflammatory capacity ( $p=0.003$ ) following *ex vivo* PMA/ionomycin stimulation, a finding not seen in CD4 $^{+}$  T cells (Supplementary Figures 5L, M). Lastly, although prolonged MCD diet feeding of mice housed at Tn increased the hepatic expression of *Col1a1* ( $p=0.02$ ) and *Col1a2* ( $p=0.01$ ) (Supplementary Figure 4N), such induction did not yield robust histological differences in hepatic fibrosis at the conclusion of the study (Supplementary Figure 5E).

### Tn housing restricts WD+CCl<sub>4</sub> driven liver disease pathogenesis

Carbon tetrachloride (CCl<sub>4</sub>) is a prominent hepatotoxin known to drive robust hepatic inflammation, damage, and fibrosis (9, 40, 42, 43). Thus, we next examined how Tn housing shapes CCl<sub>4</sub> treatment-driven liver damage. C57BL/6 wild type mice were housed at Tn and Ts and treated with CCl<sub>4</sub> i.p. 2 times a week for 3 weeks (Supplementary Figure 6A). Both Tn and Ts housed mice treated

with CCl<sub>4</sub> had similar body weights at the conclusion of the study (Supplementary Figure 6B) and hepatic immune cell accrual that correlated with extensive hepatocellular necrosis (Supplementary Figures 6C, D, see yellow arrows). However, despite similar disease pathology, Tn housed mice treated with CCl<sub>4</sub>, compared to Ts housed counterparts, had reduced ALT levels ( $p=0.001$ ) (Supplementary Figure 6E). In addition, CCl<sub>4</sub> treatment induced comparable hepatic *Tnfα* and *Ccl2* and *Ccl3* expression in both Tn and Ts housed mice (Supplementary Figures 6F, G), similar hepatic immune cell accrual (Supplementary Figures 6H, I), and hepatic immune cell inflammatory capacity following *ex vivo* stimulation with PMA/ionomycin (Supplementary Figures 6J, K). CCl<sub>4</sub> is also a potent driver of hepatic fibrosis. Analysis of the whole liver tissue showed similar expression of fibrosis associated genes (*Col1a1*, *Col1a2* and *Acta2*) (Supplementary Figure 6L) in Tn and Ts housed mice treated with CCl<sub>4</sub>, which also correlated with similar induction of sinusoidal fibrosis as determined by histopathological analyses (Supplementary Figure 6M).

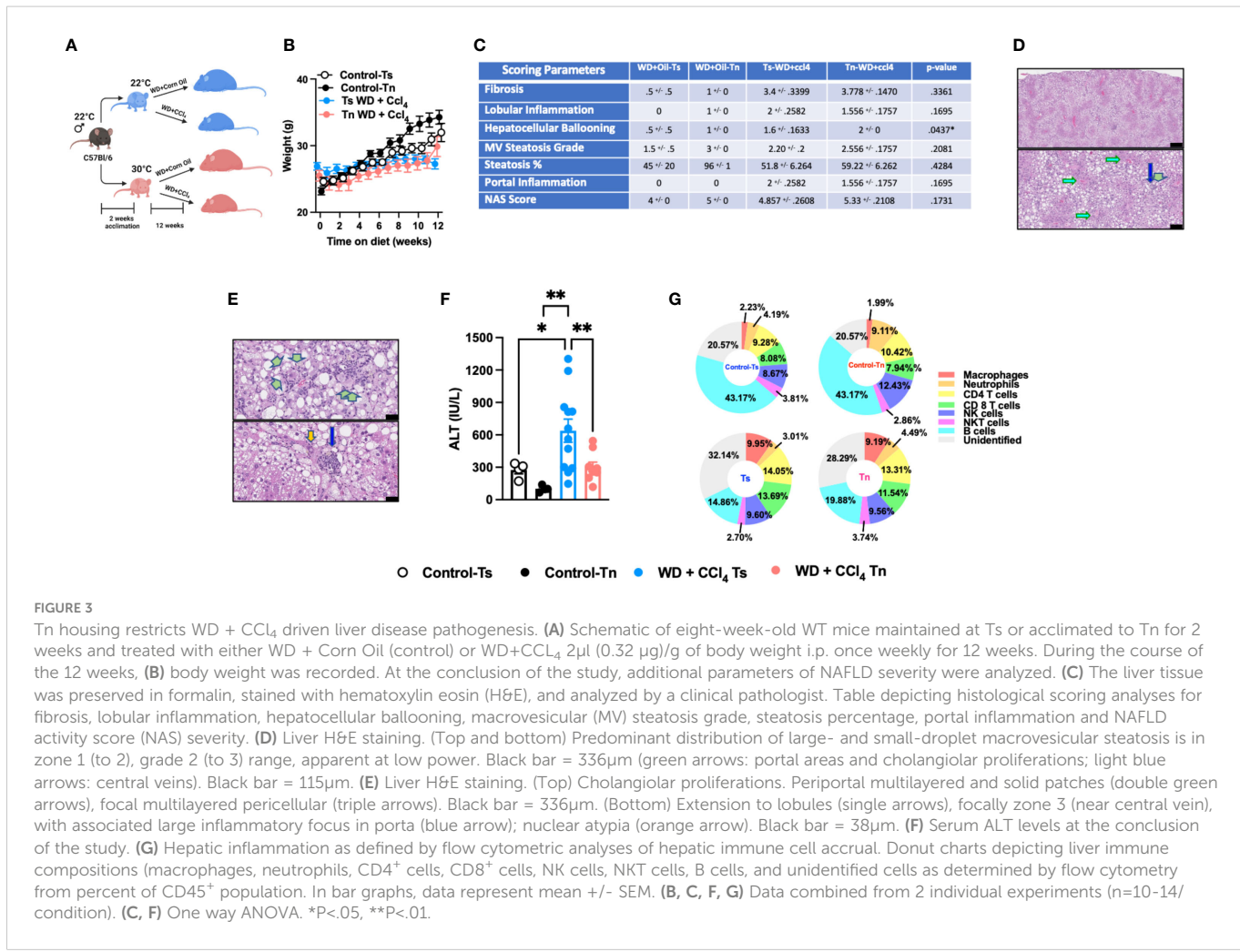
Western Diet (WD) feeding coupled with low dose CCl<sub>4</sub> administration (WD+CCl<sub>4</sub>) more accurately recapitulates the histopathological manifestations of NASH with progression to cirrhosis (5). Hence, C57BL/6 wild type mice housed at Tn and Ts conditions were fed a WD coupled with low dose of CCl<sub>4</sub>

administration for 12 weeks (Figure 3A). Tn housing did not impact total body weight gain over time (Figure 3B), wet liver weights or hepatic triglyceride accumulation (Supplementary Figures 7A, B). Congruently, Tn housed mice receiving WD+CCl<sub>4</sub>, compared to Ts housed counterparts, had similar distribution of small droplet macrovesicular steatosis and large droplet macrovesicular steatosis (Figures 3C, D, see arrows). Additional histopathological analyses revealed that Tn housed, WD+CCl<sub>4</sub> treated mice had increased hepatocellular ballooning ( $p=0.04$ ), but similar distribution of inflammatory foci and similar overall NAS severity (Figures 3C, E, see green arrows). Similarly, to CCl<sub>4</sub> treatment alone, Tn housed, WD+CCl<sub>4</sub> treated mice exhibited decreased serum ALT ( $p=0.01$ ) but not AST levels (Figure 3F and Supplementary Figure 7C). Tn housed, WD+CCl<sub>4</sub> treated mice, compared to Ts housed counterparts, also had increased hepatic *Tnfa*, ( $p=0.03$ ) *Ccl2* ( $p=0.007$ ) and *Ccl3* ( $p=0.02$ ) expression (Supplementary Figures 7D, E). Subsequent analyses of the immune cell composition revealed Tn housing coupled to WD+CCl<sub>4</sub> treatment decreased absolute number of hepatic immune cells ( $p=0.05$ ) (Supplementary Figure 7F), most prominently in the macrophage compartment ( $p=0.03$ ) (Figure 3G and Supplementary Table 3). Nevertheless, Tn housing did not impact macrophage inflammatory capacity but rather modified the inflammatory capacity of CD4<sup>+</sup> T cells following *ex vivo* stimulation with PMA/ionomycin ( $p=0.001$ ) (Supplementary Figures 7G, H). We next

examined if Tn housing modified WD + CCl<sub>4</sub> treatment driven hepatic fibrosis. Increased hepatic expression of fibrosis (*Col1a1*, ( $p=0.31$ ) *Col1a2* ( $p=0.51$ ), *Acta2* ( $p=0.05$ )), cell regeneration (*Ccnd1* ( $p=0.002$ ) and *Ki67* ( $p=0.0005$ )) and HCC-associated genes (*Afp* ( $p=0.009$ ) and *H19* ( $p=0.12$ )) was observed in Tn housed, WD + CCl<sub>4</sub> treated mice, compared to Ts housed counterparts (Supplementary Figures 7I, K). Nonetheless, robust histological differences in pericellular delicate fibrosis (see green arrows) or HCC development as indicated by similar presence of nuclear atypia (see yellow ovals) at the conclusion of the study were not observed (Supplementary Figure 7L). Lastly, as in other experimental models of NAFLD (Figures 1 and 2), Tn housing did not modify hepatic expression of insulin signaling (*Pparγ* and *Irs1*) or lipid metabolism-associated genes (*Lxra*, *Lipe*, *Chrebp*, and *Srebp*) (Supplementary Figures 7M, N).

## Discussion

In this comparative study, we built upon our previous findings that demonstrated the ability of Tn housing (which allows for physiological responses to inflammatory stimuli) to modify key inflammatory responses associated with HFD driven NAFLD development and progression. Here we add to that knowledge by



showing that Tn housing also modifies liver disease hallmarks in multiple experimental mouse models of NAFLD.

HFD feeding is favored in experimental models of NAFLD as it induces robust obesity, obesity-associated metabolic sequelae, and hepatic steatosis. However, a major shortcoming of this model is that even prolonged feeding does not induce severe steatohepatitis or hepatic fibrosis (40, 44). NASH diet is composed of high fat content coupled to high content of carbohydrates – a dietary composition that more accurately mimics human dietary intakes and is believed to more closely recapitulate NAFLD development progression. However, an apparent caveat of this model is that the higher cholesterol content is overwhelming and does not represent physiological levels found in human diets (45). Overnutrition, commonly seen in diet induced obesity models, significantly alters cellular metabolism (46). Altered cellular metabolism profoundly shapes immune cell function (24, 46). Specifically, in the context of NAFLD, obesity drives ectopic fat deposition into the liver and subsequent immune cell infiltration (47, 48). Our findings demonstrate that Tn housing was sufficient to augment obesity, ALT, hepatic immune cell accrual and the overall liver tissue damage in during NASH diet feeding. Specifically, we demonstrate that Tn housing was sufficient to not only promote increased obesity over time but to also increase hepatic accrual of macrophages and neutrophils which correlates with elevated ALT and the overall NAS severity. However, the signaling mechanisms shaping the altered NAFLD kinetics and severity under Tn housing conditions that uniquely promote increased hepatic myeloid cell accrual remain unknown. During NASH/NAFLD, liver resident macrophages (Kupffer cells) decrease and are replaced by recruited circulating monocyte-derived macrophages. These macrophages are distinct from Kupffer cells, and their presence is associated with worsened liver disease (49). If and how Tn housing modifies the recruitment of these distinct macrophage populations and their functional capabilities is unknown. In addition, investigation of the impact of Tn housing on environmental cues or other non-immune cell factors which may contribute to worsened disease pathogenesis is warranted. Tn housing was not sufficient to induce hepatic fibrosis under NASH diet feeding conditions. Hence, future studies should focus on the role of Tn housing on activation of other liver resident cells known to contribute to fibrosis development including stellate cells (50). Additionally, the contribution of other immune cells to hepatic inflammation and fibrosis outside the scope of this study should be investigated (51–54).

Although MCD diet induces robust hepatic steatosis, inflammation, and fibrosis, a major disadvantage of this model is that it induces chronic weight loss and lacks the presence of metabolic syndrome – parameters frequently associated with obesity-driven liver disease in humans. However, given the increase in cases of non-obese individuals with NAFLD or “lean NAFLD,” this model is again garnering more attention (55, 56). Notably, lean ( $BMI < 25\text{kg}/\text{m}^2$ ) and non-obese ( $BMI < 30\text{kg}/\text{m}^2$ ) individuals with NAFLD make up 5.1% and 12.1% of all NAFLD cases respectively in the general population (57). These individuals, in addition to liver disease, display worse type 2 diabetes, metabolic syndrome, cardiovascular disease, and fibrosis compared to their obese counterparts (58, 59). Such reports seemingly uncouple obesity from NAFLD and validate the use of MCD as a tool to understand disease progression in “lean NAFLD.”

We show that Tn housing in context of MCD diet was sufficient to amplify hepatic steatosis, hepatocellular ballooning, lobular inflammation, overall NAS severity, and hepatic fibrosis. Moreover, these effects were amplified under Tn conditions after prolonged exposure to MCD diet feeding. However, we did not observe differences in fibrosis during prolonged MCD diet exposure. Given that observed reduction in macrophage inflammation under these conditions, prolonged exposure to MCD-driven NAFLD milieu could contribute to immune cell exhaustion and diminished hepatic fibrosis (60). Notably, combined deficiency of choline and methionine impairs  $\beta$ -oxidation and decreases secretion of VLDL contributing to increased fatty liver, cytokine secretion, inflammation, and development of fibrosis (9). Additionally,  $\beta$ -oxidation regulates immune cell inflammation and function (26, 61, 62). If and how Tn housing regulates  $\beta$ -oxidation, subsequent immune responses and VLDL secretion remains unknown.

Chemicals such as  $CCl_4$  are effective triggers of hepatic fibrosis and have been heavily utilized to study liver disease progression. Cellular toxicity, a major caveat of this method, is known to induce generation of reactive metabolites, ROS, oxidative stress and imbalances in cellular damage and regeneration. These processes can subsequently activate hepatic stellate cell proliferation and induce development and progression of hepatic fibrosis (42, 63). We show that both Tn and Ts housing in the context of high dose  $CCl_4$  administration drive similar hepatocellular necrosis and fibrosis. Despite the histopathological similarities, Tn housing blunted systemic ALT level. ALT, abundantly found in the cytosol of hepatocytes, is released upon hepatocellular damage and has a half-life of approximately 47 hours in the blood, with levels varying 10–30% within a given day (64). Whether the ALT levels are attributed to altered cycles of hepatocellular regeneration under Ts and Tn housing conditions remains unknown. Housing temperature also regulates inflammatory signaling cascades (e.g., NF- $\kappa$ B, TNF $\alpha$ , IL-6) that drive the initial priming necessary to stimulate hepatocyte regeneration (65). As such, the contribution of Tn housing to hepatocellular damage and regeneration in the context of  $CCl_4$  treatment warrants further investigation. Additionally, although ALT is often recognized as reliable marker of liver disease, ALT levels do not always directly correlate with disease progression. In the context of hepatitis B and C infection, some individuals display normal ALT levels even with the presence of advanced fibrosis (66, 67). As such, despite the invasive nature of the procedure, liver biopsy remains the gold standard in determining NAFLD diagnosis and disease severity.

Recently, low dose  $CCl_4$  in combination with WD feeding (containing cholesterol) is utilized to induce hepatic fibrosis and mimic human NASH in C57BL/6 wild type mice – a process uncharacteristic of WD feeding alone (5). Diet induced obesity is a known modifier of hepatic immune cell accrual including macrophages, which is further exacerbated under Tn housing conditions. Interestingly, in the context of Tn housing our data shows a reduction in total hepatic macrophage accrual in WD +  $CCl_4$  treated mice.  $CCl_4$  treatment modifies immune cell function (43, 68). How Tn housing modulates hepatic immune cell function during WD+ $CCl_4$  combination remains to be studied. Although no differences in histological fibrosis were observed, increased expression of fibrosis, cell proliferation and HCC-associated genes under Tn conditions was noted. These data suggest that prolonged exposure

may be needed to fully uncover Tn housing mediated WD+CCl<sub>4</sub> treatment effects on fibrosis. Overall, our findings with WD+CCl<sub>4</sub> agree with published reports (5), apart from serum ALT analysis. We show that WD+CCl<sub>4</sub> elevates serum ALT in Ts conditions over the control group (WD+Oil). This could be due in part to differences in host gut microbiome, time of day of serum collection or hepatocellular cycles of damage and regeneration (69–71). In the context of Tn housing, we demonstrate that WD+CCl<sub>4</sub> treatment blunts ALT levels. These data suggest that under Tn conditions the WD feeding may contribute to activation of other mechanisms subsequently offering some protection against the observed increased ALT seen in Ts housed counterparts. However, it should be noted that hepatic histopathological manifestations due to CCl<sub>4</sub> use are not consistent with NAFLD histopathology seen in humans. Hence, these key limitations should be accounted for when using CCl<sub>4</sub> to model NAFLD associated histopathology.

The molecular mechanisms that contribute to NAFLD progression are still under investigation. Steatosis development is due in part to both extra- and intrahepatic processes. Hormone sensitive lipase (HSL) regulates adipose tissue TG hydrolysis into free fatty acids (FFAs) which are subsequently taken up by the liver (72, 73). Insulin inhibits HSL activity during feeding, hence during the low insulin fasting state HSL activity is increased and facilitates fatty acid release (72). Indeed, inhibition of HSL in mice decreases plasma FFA concentration and reduces hepatic steatosis (72, 74). Additionally, rest (i.e., non-exercise conditions) prompts fatty acid (FA) release and creates an imbalance of FAs in circulation versus their rate of oxidation. In our studies no significant changes in hepatic HSL (*Lipe*) or insulin signaling activity (*Irs1* and *Pparγ*) between Ts and Tn housed groups were observed. These data suggests that Tn housing does not dominantly impact TG hydrolysis into FFA and subsequent uptake by the liver contributing to hepatic steatosis. It may be that lipoprotein lipase (LPL), which regulates intravascular hydrolysis of plasma chylomicron and very low-density lipoprotein (VLDL) into FAs for subsequent uptake by the adipose tissue and the liver, may be modified by Tn housing (72). In fact, in experimental models of atherosclerosis Tn housing has been shown to alter low-density lipoprotein composition (15). However, given limited changes in expression of insulin signaling genes between Ts and Tn housed groups in our models (something that promotes LPL activity (72), such studies require further investigation. Intrahepatic perturbation in lipid metabolic processes can also regulate hepatic steatosis. High sucrose feeding has been shown to promote steatosis *via de novo* lipogenesis. Moreover, inhibition of glucose-6-phosphatase causes hepatic entrapment of glucose and subsequently promotes *de novo* lipogenesis and hepatic steatosis. Indeed, carbohydrate-responsive element-binding protein (*Chrebp*) is activated by glucose and promotes *de novo* lipogenesis (75). Yet, our data does not uncover differences in *Chrebp* between Ts and Tn housed groups. Analysis of other genes known to regulate lipid lipogenesis including sterol regulatory element binding protein and liver x receptors (*Srebp* and *Lxra*) (76, 77) similarly did not reveal difference in expression between Ts and Tn housed groups. Collectively, these studies may suggest that Tn housing possibly regulates development of hepatic steatosis *via* novel mechanisms. Of note, dietary insults may regulate DNA methylation which heavily relies on S-adenosylmethionine (SAM) availability and methyl donors from foods. Deficiency in

folate, one of such methyl donors, is known to contribute to hepatic triglyceride accumulation *via* regulation of fatty acid synthesis genes (78, 79). Thus, whether Tn housing modifies diet associated regulation of epigenetic mechanisms contributing to NAFLD is underdefined.

Housing temperature exerts profound effects in shaping immune responsiveness. Cold stress is associated with norepinephrine release, activation of beta-adrenergic receptors on immune cells and subsequent regulation of immune cell function (80). In the context of HFD driven NAFLD, Tn housing significantly lowered expression of genes central to glucocorticoid receptor (GR) and beta 3 adrenergic receptor signaling. Moreover, Tn housing resulted in lower serum concentrations of the immunosuppressive glucocorticoid corticosterone and expression of genes that inhibit inflammation (*GR and beta 2 adrenergic receptor (β2AR)* in the spleen (3)). Notably, immune cells deficient in GR or β2AR exhibit exacerbated inflammatory cytokine production following LPS stimulation (81, 82). Additionally, sequencing of peripheral blood mononuclear cells from Ts and Tn housed mice showed that Tn housing promoted increased expression of genes that negatively regulate immune responses (3). Whether the same mechanisms are conserved in other experimental models of NAFLD remains underdefined and should be examined.

Temperature modifies epigenetic regulation of immune response. It has been reported that optimally (25°C) challenged fish displayed increased IgM<sup>+</sup> B cell secretion, macrophage inflammation and recovery following viral infection compared to sub-optimally (17°C) challenged fish. Notably, fish that survived infection during a suboptimal challenge exhibited significantly increased H3 and H4 histone modifications compared to that of optimally challenged fish. Specifically, they found that suboptimal challenge resulted in H3K9ac displaying transcriptional competency, activation of trained immunity H3K4me3, and enrichment of H3 histone-lysine 4 mono-methylation (H3K4me1), and a robust re-stimulatory immune response. Essentially, all assayed H4 modifications were significantly higher in sub-optimally challenged infected fish compared to optimally challenged infected fish. Moreover, these fish had more methylation along cytosine residues compared to optimally challenged fish, suggesting the role of epigenetics and subsequent activation of trained immunity in convalescing sub optimally challenged fish (83). Thus, temperature may act as a potent regulator of epigenetic mechanisms contributing to regulation of immune responses during viral infection. Whether Tn housing modifies epigenetic activity in murine immune cells and their contribution to NAFLD pathogenesis represents an attractive area of investigation.

Febrile response to infection is preserved in mammals with evidence invoking existence of beneficial response to infection (84). In fact, the available data suggests that an elevated temperature (37.5° C to 39.4°C) in ICU patients is associated with better outcomes to infectious insult compared to normothermia or hyperthermia (above 40°C) (84–86). In elderly, increased pneumonia related mortality is observed in those who lacked fever (29%) compared to those who developed a febrile response (4%). Thus, these data suggests that internal temperatures may indeed impact the immune response or slow pathogen virulence. However, there is insufficient data to determine the impact of environmental temperature on modulation

of immune responses and development of disease, specifically NAFLD, under steady state conditions in humans. Importantly, divergence in dietary consumption and lifestyle among various populations, given its relevance to NAFLD development, represents a key obstacle in addressing the impact of temperature on NAFLD severity in humans. Hence, additional epidemiological studies are required across various geographical landscapes to begin to draw correlations between NAFLD prevalence and climate.

In summary, our data demonstrates that Tn housing modifies hepatic immune cell accrual, lobular inflammation, fibrosis and overall amplifies liver tissue damage severity in experimental models of NAFLD in mice. Specifically, we demonstrate that Tn housing modifies hepatic immune cell inflammation across all models studied. Further investigation is required to complete in depth characterization of immune cell subsets and their genomic and transcriptional landscapes. These data are relevant for future comparisons of immune response in experimental models with human disease. Thus, the utility of thermoneutral housing as a means of modeling physiological murine immune responses to various inflammatory stimuli is becoming more recognized. Together, the initial findings of our studies when coupled to future investigation on this topic might serve as a foundation for interrogating how Tn housing instructs immune cell function in the context of liver inflammation and disease in multiple settings. Collectively, these insights may allow for the development of future therapies to NAFLD *via* improved understandings of immune mechanisms underlying disease development and progression.

## Data availability statement

The original contributions presented in the study are included in the article/[Supplementary Material](#). Further inquiries can be directed to the corresponding author.

## Ethics statement

The animal study was reviewed and approved by Cincinnati Children's Hospital Medical Center IACUC.

## Author contributions

JO, MM-F, DG and SD contributed to conception and design of the study. JO, KS, DG, PA, MD, MM-F, and TS executed the experimental plan and contributed to subsequent data analyses. JO, KS, and DG performed the data and statistical analyses. SS performed histological scoring and analyses. JO, KS, MM-F and SD wrote the manuscript. All authors contributed to the article and approved the submitted version.

## Funding

This work was supported in part by NIH R01DK099222, Department of Defense (DoD) W81XWH2010392, American

Diabetes Association (ADA) 1-18-IBS-100, CCHMC Pediatric Diabetes and Obesity Center, and CCRF Endowed Scholar Award (to SD); R01DK099222-08S1 (associated with SD and JO); R01DK099222-02S1 (associated with SD, and MM-F); American Heart Association (AHA) 17POST33650045 and ADA 1-19-PMF-019 (to MM-F); NIH 1F31AI169757-01 (associated with PA); and PHS Grant P30 DK078392 Pathology of the Digestive Disease Research Core Center at CCHMC (associated with SD).

## Acknowledgments

Images and figures were generated using [biorender.com](#).

## Conflict of interest

The authors declare that the research was conducted in the absence of any commercial or financial relationships that could be construed as a potential conflict of interest.

## Publisher's note

All claims expressed in this article are solely those of the authors and do not necessarily represent those of their affiliated organizations, or those of the publisher, the editors and the reviewers. Any product that may be evaluated in this article, or claim that may be made by its manufacturer, is not guaranteed or endorsed by the publisher.

## Supplementary material

The Supplementary Material for this article can be found online at: <https://www.frontiersin.org/articles/10.3389/fimmu.2023.1095132/full#supplementary-material>

### SUPPLEMENTARY FIGURE 1

Tn housing does not impact liver damage in chow mice. Eight-week-old WT mice were fed a chow diet and housed at Ts or Tn for 24 weeks. During the course of the 24 weeks, (A) body weights were recorded. At the conclusion of the study, (B) wet liver weights were recorded, and (C) serum ALT levels were measured. In bar graphs, data represent mean + SEM. Representative of 3 individual experiments (n=8/condition). (A–C) Student's t-test. \*\*P<0.001.

### SUPPLEMENTARY FIGURE 2

Related to Main Figure 1: Characterization of liver disease in Ts and Tn housed NASH diet fed mice. At the conclusion of the study, additional parameters of NAFLD severity were analyzed. (A) Wet weights of epididymal, inguinal and perirenal white adipose tissues, and (B) wet liver weights. (C) Hepatic triglycerides levels measured in homogenized tissue lysates. (D–H) Hepatic inflammation as defined by gene expression and hepatic immune cell accrual and inflammatory cytokine production at the conclusion of the study. qPCR analysis of liver (D) *Tnfa* and (E) *Ccl2* and *Ccl3* expression. (F) Absolute numbers of hepatic immune cells quantified via hemacytometer. (G, H) Hepatic immune cells were stimulated for 4 hours with Phorbol 12-myristate 13-acetate (PMA; 50 ng/ml) and Ionomycin (1 µg/ml), in presence of Brefeldin A (10 µg/ml) and analyzed for cytokine production by flow cytometry. (G) Frequency of F4/80<sup>+</sup>CD11b<sup>hi</sup>TNF<sup>+</sup> expressing cells and (H) frequency of CD4<sup>+</sup>TNF<sup>+</sup>, CD4<sup>+</sup>IFNg, and CD4<sup>+</sup>IL-17a<sup>+</sup> cells. (I, J) Quantification of hepatic fibrosis. qPCR analysis of liver (I) *Col1a1*, *Col1a2*, and *Acta2* expression. (J) (Top and Bottom) Steatosis on trichrome stain, with no pericentral or periportal fibrosis, inflammation or cholangiolar proliferations. Top, black bar = 39µm. Bottom,

black bar = 42 $\mu$ m. (K, L) Quantification of insulin signaling and lipid metabolism-associated genes in the liver. qPCR analysis of liver (K) *Pparg* and *Irs1*, (L) *Chrebp*, *Srebp*, *Lxra* and *Lipe* expression. In bar graphs, data represent mean +/- SEM. Representative of 2 individual experiments (n=4–6/condition). (A) and (C–E) and (G–I) One-way ANOVA. \*P<0.05, \*\*P<0.01 \*\*\*P<0.001, \*\*\*\*P<0.0001. (B, F) and (I, K–L) Student's t-test. \*P<0.05, \*\*P<0.01, \*\*\*P<0.001, \*\*\*\*P<0.0001

#### SUPPLEMENTARY FIGURE 3

Related to Main Figure 1: A representative plots of flow cytometry gating strategy of hepatic immune cells. Liver infiltrated immune cells were isolated as described in the materials and methods section. Single cell suspensions were stained with viability dye and surface markers antibody cocktail for 30 minutes at 4°C. Cells were then washed in PBS + 2% FBS and then prepared for reading on cytometer. A minimum of 200,000 cells were recorded in each tube.

#### SUPPLEMENTARY FIGURE 4

Related to Main Figure 2: Characterization of liver disease in Ts and Tn housed mice on short-term MCD diet. At the conclusion of the study, additional parameters of NAFLD severity were analyzed. (A) Liver to body weight ratio was quantified and (B) hepatic triglyceride levels were measured in homogenized tissue lysates. (C) Hepatocellular damage as quantified by serum AST levels collected at the conclusion of the study. (D–H) Hepatic inflammation as defined by gene expression and hepatic immune cell accrual and inflammatory cytokine production at the conclusion of the study. qPCR analysis of liver (D) *Tnfa* and (E) *Ccl2* and *Ccl3* expression. (F) Absolute number of hepatic immune cells were quantified using a hemacytometer. (G, H) Hepatic immune cells were stimulated for 4 hours with Phorbol 12-myristate 13-acetate (PMA; 50 ng/ml) and lonomycin (1  $\mu$ g/ml), in presence of Brefeldin A (10  $\mu$ g/ml) and analyzed for cytokine production by flow cytometry. (G) Frequency of F4/80<sup>+</sup>CD11b<sup>hi</sup>TNF $\alpha$ <sup>+</sup> expressing cells and (H) frequency of CD4<sup>+</sup>TNF $\alpha$ <sup>+</sup>, CD4<sup>+</sup>IFNg, and CD4<sup>+</sup>IL-17a<sup>+</sup> cells. (I) Quantification of hepatic fibrosis. qPCR analysis of liver *Col1a1*, *Col1a2*, and *Acta2* expression. (J, K) Quantification of insulin signaling and lipid metabolism-associated genes in the liver. qPCR analysis of liver (J) *Pparg* and *Irs1*, and (K) *Chrebp*, *Srebp*, *Lxra* and *Lipe* expression. In bar graphs, data represent mean +/- SEM. (A–K) Data combined from 2 individual experiments, (n=8/condition). (A–D) and (F–H) One-way ANOVA. \*P<0.05, \*\*P<0.01 \*\*\*P<0.001, \*\*\*\*P<0.0001. (I–K) Student's t-test. \*P<0.05, \*\*P<0.01, \*\*\*P<0.001.

#### SUPPLEMENTARY FIGURE 5

Related to Main Figure 2: Characterization of Ts and Tn housed mice on prolonged MCD diet. (A) Schematic of experimental design. Eight-week-old WT mice maintained at Ts or acclimated to Tn for 2 weeks and fed a chow (baseline reference) or MCD diet for 10 weeks. During the course of the 10 weeks (B) body weight was recorded. At the conclusion of the study, additional parameters of NAFLD severity were analyzed. (C) Liver to body weight ratio was recorded, (D) hepatic triglyceride levels were measured in homogenized tissue lysates and (E) hepatocellular damage was quantified by serum ALT and (F) AST levels. (G) The liver tissue was preserved in formalin, stained with hematoxylin eosin (H&E), and analyzed by a clinical pathologist. Table depicting histological scoring analyses for fibrosis, lobular inflammation, hepatocellular ballooning, macrovesicular (MV) steatosis grade, steatosis percentage, portal inflammation and NAFLD activity score (NAS) severity. (H–M) Hepatic inflammation as defined by gene expression and hepatic immune cell accrual and inflammatory cytokine production at the conclusion of the study. qPCR analysis of liver (H) *Tnfa* and (I) *Ccl2* and *Ccl3* expression. (J) Absolute number of hepatic immune cells were calculated using a hemacytometer. (K–M) Hepatic inflammation as defined by flow cytometric analyses of hepatic immune cell accrual. (K) Donut charts depicting liver immune compositions (macrophages, neutrophils, CD4<sup>+</sup> cells, CD8<sup>+</sup> cells, and unidentified cells) as determined by flow cytometry. Cells were stimulated for 4 hours with Phorbol 12-myristate 13-acetate (PMA; 50 ng/ml) and lonomycin (1  $\mu$ g/ml), in presence of Brefeldin A (10  $\mu$ g/ml) and analyzed for cytokine production. (L) Hepatic frequency of F4/80<sup>+</sup>CD11b<sup>hi</sup>TNF $\alpha$ <sup>+</sup> expressing cells and (M) hepatic frequency of CD4<sup>+</sup>TNF $\alpha$ <sup>+</sup>, CD4<sup>+</sup>IFNg, and CD4<sup>+</sup>IL-17a<sup>+</sup> cells. (N) Quantification of hepatic fibrosis by qPCR analysis using *Col1a1*, *Col1a2* and *Acta2* expression. In bar graphs, data represent mean +/- SEM. For box plots, the midline represents the mean, boxes represent the interquartile range. (B–N) Data combined from 2 independent experiments (n=6–8/condition). (C, D) and (F–H) and (J–M) One-way ANOVA. \*P<0.05, \*\*P<0.01 \*\*\*P<0.001. One-way ANOVA. \*P<0.05, \*\*P<0.01. (I, N) Student's t-test. \*P<0.05, \*\*P<0.01.

#### SUPPLEMENTARY FIGURE 6

Tn housing decreases hepatocellular ALT release in CCl<sub>4</sub> model of liver injury. (A) Schematic of experimental design. Eight-week-old WT mice maintained at Ts or acclimated to Tn for 2 weeks and treated with either olive oil (vehicle control) or CCl<sub>4</sub> i.p. 2x weekly for 3 weeks. (B) Terminal body weight recorded at the conclusion of the study. (C, D) The liver tissue was preserved in formalin, stained with hematoxylin eosin (H&E), and analyzed by a clinical pathologist. (C) Table depicting histological scoring analyses for fibrosis, lobular inflammation, hepatocellular ballooning, macrovesicular (MV) steatosis grade, steatosis percentage, portal inflammation and NAFLD activity score (NAS) severity. (D) Liver H&E staining. (Top) Immune cell infiltrate. Black bar = 82 $\mu$ m. (Bottom) Hepatocellular necrosis as indicated by acidophil bodies (yellow arrows). Black bar = 52 $\mu$ m. (E) Hepatocellular damage as quantified by serum ALT levels collected at the conclusion of the study. (F–K) Hepatic inflammation as defined by gene expression and hepatic immune cell accrual and inflammatory cytokine production at the conclusion of the study. qPCR analysis of liver (F) *Tnfa* and (G) *Ccl2* and *Ccl3* expression. (H) Absolute number of hepatic immune cells were calculated using a hemacytometer. (I) Donut charts depicting liver immune compositions (macrophages, neutrophils, CD4s, CD8s, NKs, NKTs, B cells, and unidentified cells) as determined by flow cytometry from percent of CD45<sup>+</sup> population. (J, K) Cells were stimulated for 4 hours with Phorbol 12-myristate 13-acetate (PMA; 50 ng/ml) and lonomycin (1  $\mu$ g/ml), in presence of Brefeldin A (10  $\mu$ g/ml) and analyzed for cytokine production by flow cytometry. (J) Hepatic frequency of F4/80<sup>+</sup>CD11b<sup>hi</sup>TNF $\alpha$ <sup>+</sup> and (K) hepatic frequency of CD4<sup>+</sup>TNF $\alpha$ <sup>+</sup>, CD4<sup>+</sup>IFNg, and CD4<sup>+</sup>IL-17a<sup>+</sup> cells. (L, M) Quantification of hepatic fibrosis. qPCR analysis of liver (L) *Col1a1*, *Col1a2* and *Acta2* expression. (M) (Top) Trichrome staining. Zone 3, hepatocellular necrosis with inflammation and fibrosis. Black bar = 256 $\mu$ m. (Bottom) On left side, hepatocellular necrosis with pericellular fibrosis and inflammation, imparting a stellate outline; scattered foamy macrophages. On right side, hepatocytes preserved in zone 1. Black bar = 35 $\mu$ m. In bar graphs, data represent mean +/- SEM. (B, E–L) Data combined from 2 individual experiments (n=7–8/condition). (C–D, M) Data combined from 2 individual experiments (n=3–4/condition). (E, F, H) and (J, K) One-way ANOVA. \*\*P<0.01. (G, L) Student's t-test. \*P<0.05, \*\*P<0.01.

#### SUPPLEMENTARY FIGURE 7

Related to Main Figure 3: Characterization of liver disease in Ts and Tn housed mice during WD+CCl<sub>4</sub> treatment. At the conclusion of the study, additional parameters of NAFLD severity were analyzed. (A) Wet liver weights were recorded at the conclusion of the study and (B) hepatic triglyceride levels were measured in homogenized tissue lysates. (C) AST levels were measured in the serum. (D–H) Hepatic inflammation as defined by gene expression and hepatic immune cell accrual and inflammatory cytokine production at the conclusion of the study. qPCR analysis of liver (D) *Tnfa* and (E) *Ccl2* and *Ccl3* expression. (F) Absolute number of hepatic immune cells was calculated using a hemacytometer. (G, H) Hepatic inflammation as defined by flow cytometric analyses of hepatic immune cell accrual. Isolated hepatic immune cells were stimulated for 4 hours with Phorbol 12-myristate 13-acetate (PMA; 50 ng/ml) and lonomycin (1  $\mu$ g/ml), in presence of Brefeldin A (10  $\mu$ g/ml) and analyzed for cytokine production. (G) Hepatic frequency of F4/80<sup>+</sup>CD11b<sup>hi</sup>TNF $\alpha$ <sup>+</sup> expressing cells and (H) hepatic frequency of CD4<sup>+</sup>TNF $\alpha$ <sup>+</sup>, CD4<sup>+</sup>IFNg, and CD4<sup>+</sup>IL-17a<sup>+</sup> cells. (I) Quantification of hepatic fibrosis using qPCR analysis of liver *Col1a1*, *Col1a2* and *Acta2* expression. (J) Quantification of hepatocellular regeneration using qPCR analysis of liver *Ki67* and *Ccnd1* expression. (K) Quantification of hepatocellular carcinoma genes using qPCR analysis of liver *H19* and *Afp* expression. (L) Liver hematoxylin and eosin (H&E) staining. (Top) Bile ductular (cholangiolar) proliferations with associated pericellular delicate fibrosis apparent in the right side of the field. Black bar = 332 $\mu$ m. (Bottom) Nuclear inclusions (including in binucleated forms) (orange arrows), nuclear atypia overlapping with patterns of steatosis (yellow ovals), in zone 3, in a background of cholangiolar proliferations. Black bar = 31 $\mu$ m. (M, N) Quantification of insulin signaling and lipid metabolism-associated genes in the liver. qPCR analysis of liver (M) *Pparg* and *Irs1* and (N) *Chrebp*, *Srebp*, *Lxra* and *Lipe* expression. In bar graphs, data represent mean +/- SEM. (A–D) Data combined from 2 individual experiments (n=10/condition) (E, I–J) Data combined from 2 individual experiments (n=7–8/condition). (F) Data combined from 2 individual experiments (n=10–14/condition) (G, H) Data combined from 2 individual experiments (n=6/condition). (M, N) Data combined from 2 individual experiments (n=10–11/condition). (A–H) One-way ANOVA. \*P<0.05, \*\*P<0.005, \*\*\*P<0.001, \*\*\*\*P<0.0001. (I, K) and (M, N) Student's t-test. \*P<0.05, \*\*P<0.01, \*\*\*P<0.001, \*\*\*\*P<0.0001.

## References

- Cheemerla S, Balakrishnan M. Global epidemiology of chronic liver disease. *Clin Liver Dis (Hoboken)*. (2021) 17(5):365–70. doi: 10.1002/cld.1061
- Dyson JK, Anstee QM, McPherson S. Non-alcoholic fatty liver disease: a practical approach to diagnosis and staging. *Frontline Gastroenterol* (2014) 5(3):211–8. doi: 10.1136/flgastro-2013-100403
- Giles DA, Moreno-Fernandez ME, Stankiewicz TE, Graspeuntner S, Cappelletti M, Wu D, et al. Thermoneutral housing exacerbates nonalcoholic fatty liver disease in mice and allows for sex-independent disease modeling. *Nat Med* (2017) 23(7):829–38. doi: 10.1038/nm.4346
- Rinella ME, Elias MS, Smolak RR, Fu T, Borensztajn J, Green RM. Mechanisms of hepatic steatosis in mice fed a lipogenic methionine choline-deficient diet. *J Lipid Res* (2008) 49(5):1068–76. doi: 10.1194/jlr.M800042-JLR200
- Tsuchida T, Lee YA, Fujiwara N, Ybanez M, Allen B, Martins S, et al. A simple diet- and chemical-induced murine NASH model with rapid progression of steatohepatitis, fibrosis and liver cancer. *J Hepatol* (2018) 69(2):385–95. doi: 10.1016/j.jhep.2018.03.011
- Boll M, Weber LW, Becker E, Stampfl A. Mechanism of carbon tetrachloride-induced hepatotoxicity: hepatocellular damage by reactive carbon tetrachloride metabolites. *Z Naturforsch C Biosci* (2001) 56(7–8):649–59. doi: 10.1515/znc-2001-7-826
- Ito M, Suzuki J, Tsujioka S, Sasaki M, Gomori A, Shirakura T, et al. Longitudinal analysis of murine steatohepatitis model induced by chronic exposure to high-fat diet. *Hepatol Res* (2007) 37(1):50–7. doi: 10.1111/j.1872-034X.2007.00008.x
- Christ A, Lauterbach M, Latz E. Western Diet and the immune system: An inflammatory connection. *Immunity* (2019) 51(5):794–811. doi: 10.1016/j.immuni.2019.09.020
- Van Herck MA, Vonghia L, Francque SM. Animal models of nonalcoholic fatty liver disease—a starter's guide. *Nutrients* (2017) 9(10). doi: 10.3390/nutrients910172
- Itagaki H, Shimizu K, Morikawa S, Ogawa K, Ezaki T. Morphological and functional characterization of non-alcoholic fatty liver disease induced by a methionine-choline-deficient diet in C57BL/6 mice. *Int J Clin Exp Pathol* (2013) 6(12):2683–96.
- Hirsova P, Bamidele AO, Wang H, Povero D, Revelo XS. Emerging roles of T cells in the pathogenesis of nonalcoholic steatohepatitis and hepatocellular carcinoma. *Front Endocrinol (Lausanne)*. (2021) 12:760860. doi: 10.3389/fendo.2021.760860
- Huby T, Gautier EL. Immune cell-mediated features of non-alcoholic steatohepatitis. *Nat Rev Immunol* (2022) 22(7):429–43. doi: 10.1038/s41577-021-00639-3
- Oates JR, McKell MC, Moreno-Fernandez ME, Damen M, Deep GS Jr., Qualls JE, et al. Macrophage function in the pathogenesis of non-alcoholic fatty liver disease: The macro attack. *Front Immunol* (2019) 10:2893. doi: 10.3389/fimmu.2019.02893
- Wan M, Han J, Ding L, Hu F, Gao P. Novel immune subsets and related cytokines: Emerging players in the progression of liver fibrosis. *Front Med (Lausanne)*. (2021) 8:604894. doi: 10.3389/fmed.2021.604894
- Giles DA, Ramkhelawon B, Donelan EM, Stankiewicz TE, Hutchison SB, Mukherjee R, et al. Modulation of ambient temperature promotes inflammation and initiates atherosclerosis in wild type C57BL/6 mice. *Mol Metab* (2016) 5(11):1121–30. doi: 10.1016/j.molmet.2016.09.008
- Kokolos KM, Capitano ML, Lee CT, Eng JW, Waight JD, Hylander BL, et al. Baseline tumor growth and immune control in laboratory mice are significantly influenced by subthermoneutral housing temperature. *Proc Natl Acad Sci U S A*. (2013) 110(50):20176–81. doi: 10.1073/pnas.1304291110
- Tian XY, Ganeshan K, Hong C, Nguyen KD, Qiu Y, Kim J, et al. Thermoneutral housing accelerates metabolic inflammation to potentiate atherosclerosis but not insulin resistance. *Cell Metab* (2016) 23(1):165–78. doi: 10.1016/j.cmet.2015.10.003
- Bowers SL, Bilbo SD, Dhabhar FS, Nelson RJ. Stressor-specific alterations in corticosterone and immune responses in mice. *Brain Behav Immun* (2008) 22(1):105–13. doi: 10.1016/j.bbi.2007.07.012
- Ganeshan K, Chawla A. Warming the mouse to model human diseases. *Nat Rev Endocrinol* (2017) 13(8):458–65. doi: 10.1038/nrendo.2017.48
- Bond LM, Burhans MS, Ntambi JM. Uncoupling protein-1 deficiency promotes brown adipose tissue inflammation and ER stress. *PLoS One* (2018) 13(11):e0205726. doi: 10.1371/journal.pone.0205726
- Gordon CJ. The mouse thermoregulatory system: Its impact on translating biomedical data to humans. *Physiol Behav* (2017) 179:55–66. doi: 10.1016/j.physbeh.2017.05.026
- Liu E, Lewis K, Al-Saffar H, Krall CM, Singh A, Kulchitsky VA, et al. Naturally occurring hypothermia is more advantageous than fever in severe forms of lipopolysaccharide- and escherichia coli-induced systemic inflammation. *Am J Physiol Regul Integr Comp Physiol* (2012) 302(12):R1372–83. doi: 10.1152/ajpregu.00023.2012
- Giles DA, Moreno-Fernandez ME, Stankiewicz TE, Cappelletti M, Huppert SS, Iwakura Y, et al. Regulation of inflammation by IL-17A and IL-17F modulates non-alcoholic fatty liver disease pathogenesis. *PLoS One* (2016) 11(2):e0149783. doi: 10.1371/journal.pone.0149783
- Moreno-Fernandez ME, Giles DA, Oates JR, Chan CC, Damen M, Doll JR, et al. PKM2-dependent metabolic skewing of hepatic Th17 cells regulates pathogenesis of non-alcoholic fatty liver disease. *Cell Metab* (2021) 33(6):1187–204.e9. doi: 10.1016/j.cmet.2021.04.018
- Harley IT, Stankiewicz TE, Giles DA, Softic S, Flick LM, Cappelletti M, et al. IL-17 signaling accelerates the progression of nonalcoholic fatty liver disease in mice. *Hepatology* (2014) 59(5):1830–9. doi: 10.1002/hep.26746
- Moreno-Fernandez ME, Giles DA, Stankiewicz TE, Sheridan R, Karns R, Cappelletti M, et al. Peroxisomal beta-oxidation regulates whole body metabolism, inflammatory vigor, and pathogenesis of nonalcoholic fatty liver disease. *JCI Insight* (2018) 3(6). doi: 10.1172/jci.insight.93626
- Boland ML, Oro D, Tolbol KS, Thrane ST, Nielsen JC, Cohen TS, et al. Towards a standard diet-induced and biopsy-confirmed mouse model of non-alcoholic steatohepatitis: Impact of dietary fat source. *World J Gastroenterol* (2019) 25(33):4904–20. doi: 10.3748/wjg.v25.i33.4904
- Drescher HK, Weiskirchen R, Fulop A, Hopf C, de San Roman EG, Huesgen PF, et al. The influence of different fat sources on steatohepatitis and fibrosis development in the Western diet mouse model of non-alcoholic steatohepatitis (NASH). *Front Physiol* (2019) 10:770. doi: 10.3389/fphys.2019.00770
- Kawashita E, Ishihara K, Nomoto M, Taniguchi M, Akiba S. A comparative analysis of hepatic pathological phenotypes in C57BL/6J and C57BL/6N mouse strains in non-alcoholic steatohepatitis models. *Sci Rep* (2019) 9(1):204. doi: 10.1038/s41598-018-36862-7
- Kakino S, Ohki T, Nakayama H, Yuan X, Otabe S, Hashinaga T, et al. Pivotal role of TNF-alpha in the development and progression of nonalcoholic fatty liver disease in a murine model. *Horm Metab Res* (2018) 50(1):80–7. doi: 10.1055/s-0043-118666
- Seo YY, Cho YK, Bae JC, Seo MH, Park SE, Rhee EJ, et al. Tumor necrosis factor-alpha as a predictor for the development of nonalcoholic fatty liver disease: A 4-year follow-up study. *Endocrinol Metab (Seoul)*. (2013) 28(1):41–5. doi: 10.3803/EnM.2013.28.1.41
- Koyama Y, Brenner DA. Liver inflammation and fibrosis. *J Clin Invest*. (2017) 127(1):55–64. doi: 10.1172/JCI88881
- Seki E, Schwabe RF. Hepatic inflammation and fibrosis: Functional links and key pathways. *Hepatology* (2015) 61(3):1066–79. doi: 10.1002/hep.27332
- Im YR, Hunter H, de Gracia Hahn D, Duret A, Cheah Q, Dong J, et al. A systematic review of animal models of NAFLD finds high-fat, high-fructose diets most closely resemble human NAFLD. *Hepatology* (2021) 74(4):1884–901. doi: 10.1002/hep.31897
- Teufel A, Itzel T, Erhart W, Brosch M, Wang XY, Kim YO, et al. Comparison of gene expression patterns between mouse models of nonalcoholic fatty liver disease and liver tissues from patients. *Gastroenterology* (2016) 151(3):513–25.e6. doi: 10.1053/j.gastro.2016.05.051
- Kumashiro N, Erion DM, Zhang D, Kahn M, Beddow SA, Chu X, et al. Cellular mechanism of insulin resistance in nonalcoholic fatty liver disease. *Proc Natl Acad Sci U S A*. (2011) 108(39):16381–5. doi: 10.1073/pnas.1113591108
- Pei K, Gui T, Kan D, Feng H, Jin Y, Yang Y, et al. An overview of lipid metabolism and nonalcoholic fatty liver disease. *BioMed Res Int* (2020) 2020:4020249. doi: 10.1155/2020/4020249
- Kim D, Kim WR. Nonobese fatty liver disease. *Clin Gastroenterol Hepatol* (2017) 15(4):474–85. doi: 10.1016/j.cgh.2016.08.028
- Leclerc PS, Rousseau D, Patouraux S, Guerin S, Bonnafous S, Grechez-Cassiau A, et al. MCD diet-induced steatohepatitis generates a diurnal rhythm of associated biomarkers and worsens liver injury in Klf10 deficient mice. *Sci Rep* (2020) 10(1):12139. doi: 10.1038/s41598-020-69085-w
- Machado MV, Michelotti GA, Xie G, Almeida Pereira T, Boursier J, Bohnic B, et al. Mouse models of diet-induced nonalcoholic steatohepatitis reproduce the heterogeneity of the human disease. *PLoS One* (2015) 10(5):e0127991. doi: 10.1371/journal.pone.0127991
- Jahn D, Kircher S, Hermanns HM, Geier A. Animal models of NAFLD from a hepatologist's point of view. *Biochim Biophys Acta Mol Basis Dis* (2019) 1865(5):943–53. doi: 10.1016/j.bbadiis.2018.06.023
- Dong S, Chen QL, Song YN, Sun Y, Wei B, Li XY, et al. Mechanisms of CCl4-induced liver fibrosis with combined transcriptomic and proteomic analysis. *J Toxicol Sci* (2016) 41(4):561–72. doi: 10.2131/jts.41.561
- Ikeda Y, Ohara D, Takeuchi Y, Watanabe H, Kondoh G, Taura K, et al. Foxp3+ regulatory T cells inhibit CCl4-induced liver inflammation and fibrosis by regulating tissue cellular immunity. *Front Immunol* (2020) 11:584048. doi: 10.3389/fimmu.2020.584048
- Charlton M, Krishnan A, Viker K, Sanderson S, Cazanave S, McConico A, et al. Fast food diet mouse: novel small animal model of NASH with ballooning, progressive fibrosis, and high physiological fidelity to the human condition. *Am J Physiol Gastrointest Liver Physiol* (2011) 301(5):G825–34. doi: 10.1152/ajpgi.00145.2011
- Wouters K, van Gorp PJ, Bieghs V, Gijbels MJ, Duimel H, Lutjohann D, et al. Dietary cholesterol, rather than liver steatosis, leads to hepatic inflammation in hyperlipidemic mouse models of nonalcoholic steatohepatitis. *Hepatology* (2008) 48(2):474–86. doi: 10.1002/hep.22363
- Alwarawrah Y, Kiernan K, MacIver NJ. Changes in nutritional status impact immune cell metabolism and function. *Front Immunol* (2018) 9:1055. doi: 10.3389/fimmu.2018.01055
- Kuang M, Lu S, Xie Q, Peng N, He S, Yu C, et al. Abdominal obesity phenotypes are associated with the risk of developing non-alcoholic fatty liver disease: Insights from

- the general population. *BMC Gastroenterol* (2022) 22(1):311. doi: 10.1186/s12876-022-02393-9
48. Van Herck MA, Weyler J, Kwanten WJ, Dirinck EL, De Winter BY, Francque SM, et al. The differential roles of T cells in non-alcoholic fatty liver disease and obesity. *Front Immunol* (2019) 10:82. doi: 10.3389/fimmu.2019.00082
49. Seidman JS, Troutman TD, Sakai M, Gola A, Spann NJ, Bennett H, et al. Niche-specific reprogramming of epigenetic landscapes drives myeloid cell diversity in nonalcoholic steatohepatitis. *Immunity* (2020) 52(6):1057–74.e7. doi: 10.1016/j.immuni.2020.04.001
50. Zhang CY, Yuan WG, He P, Lei JH, Wang CX. Liver fibrosis and hepatic stellate cells: Etiology, pathological hallmarks and therapeutic targets. *World J Gastroenterol* (2016) 22(48):10512–22. doi: 10.3748/wjg.v22.i48.10512
51. Bonecchi R, Facchetti F, Dusi S, Luini W, Lissandrini D, Simmelink M, et al. Induction of functional IL-8 receptors by IL-4 and IL-13 in human monocytes. *J Immunol* (2000) 164(7):3862–9. doi: 10.4049/jimmunol.164.7.3862
52. Connolly MK, Bedrosian AS, Mallen-St Clair J, Mitchell AP, Ibrahim J, Stroud A, et al. In liver fibrosis, dendritic cells govern hepatic inflammation in mice via TNF-alpha. *J Clin Invest.* (2009) 119(11):3213–25. doi: 10.1172/JCI37581
53. Novobrantseva TI, Majean GR, Amatucci A, Kogan S, Brenner I, Casola S, et al. Attenuated liver fibrosis in the absence of b cells. *J Clin Invest.* (2005) 115(11):3072–82. doi: 10.1172/JCI24798
54. Xu R, Zhang Z, Wang FS. Liver fibrosis: mechanisms of immune-mediated liver injury. *Cell Mol Immunol* (2012) 9(4):296–301. doi: 10.1038/cmi.2011.53
55. VanWagner LB, Armstrong MJ. Lean NAFLD: A not so benign condition? *Hepatol Commun* (2018) 2(1):5–8. doi: 10.1002/hep4.1143
56. Younossi ZM, Stepanova M, Negro F, Hallaji S, Younossi Y, Lam B, et al. Nonalcoholic fatty liver disease in lean individuals in the united states. *Med (Baltimore)*. (2012) 91(6):319–27. doi: 10.1097/MD.0b013e3182779d49
57. Chrysavgis L, Ztriva E, Protopapas A, Tziomalos K, Cholongitas E. Nonalcoholic fatty liver disease in lean subjects: Prognosis, outcomes and management. *World J Gastroenterol* (2020) 26(42):6514–28. doi: 10.3748/wjg.v26.i42.6514
58. Ye Q, Zou B, Yeo YH, Li J, Huang DQ, Wu Y, et al. Global prevalence, incidence, and outcomes of non-obese or lean non-alcoholic fatty liver disease: A systematic review and meta-analysis. *Lancet Gastroenterol Hepatol* (2020) 5(8):739–52. doi: 10.1016/S2468-1253(20)30077-7
59. Zou B, Yeo YH, Nguyen VH, Cheung R, Ingelsson E, Nguyen MH. Prevalence, characteristics and mortality outcomes of obese, nonobese and lean NAFLD in the united states, 1999–2016. *J Intern Med* (2020) 288(1):139–51. doi: 10.1111/joim.13069
60. Pradhan K, Yi Z, Geng S, Li L. Development of exhausted memory monocytes and underlying mechanisms. *Front Immunol* (2021) 12:778830. doi: 10.3389/fimmu.2021.778830
61. Cucchi D, Camacho-Munoz D, Certo M, Pucino V, Nicolaou A, Mauro C. Fatty acids - from energy substrates to key regulators of cell survival, proliferation and effector function. *Cell Stress.* (2019) 4(1):9–23. doi: 10.15698/cst2020.01.209
62. O'Sullivan D, van der Windt GJ, Huang SC, Curtis JD, Chang CH, Buck MD, et al. Memory CD8(+) T cells use cell-intrinsic lipolysis to support the metabolic programming necessary for development. *Immunity* (2014) 41(1):75–88. doi: 10.1016/j.jimmuni.2014.06.005
63. Fujii T, Fuchs BC, Yamada S, Lauwers GY, Kulu Y, Goodwin JM, et al. Mouse model of carbon tetrachloride induced liver fibrosis: Histopathological changes and expression of CD133 and epidermal growth factor. *BMC Gastroenterol* (2010) 10:79. doi: 10.1186/1471-230X-10-79
64. Kim WR, Flamm SL, Di Bisceglie AM, Bodenheimer HC. Public policy committee of the American association for the study of liver d. serum activity of alanine aminotransferase (ALT) as an indicator of health and disease. *Hepatology* (2008) 47(4):1363–70. doi: 10.1002/hep.22109
65. Abu Rmilah A, Zhou W, Nelson E, Lin L, Amiot B, Nyberg SL. Understanding the marvels behind liver regeneration. *Wiley Interdiscip Rev Dev Biol* (2019) 8(3):e340. doi: 10.1002/wdev.340
66. Chao DT, Lim JK, Ayoub WS, Nguyen LH, Nguyen MH. Systematic review with meta-analysis: the proportion of chronic hepatitis b patients with normal alanine transaminase <= 40 IU/L and significant hepatic fibrosis. *Aliment Pharmacol Ther* (2014) 39(4):349–58. doi: 10.1111/apt.12590
67. Sanai FM, Benmousa A, Al-Hussaini H, Ashraf S, Alhafi O, Abdo AA, et al. Is serum alanine transaminase level a reliable marker of histological disease in chronic hepatitis c infection? *Liver Int* (2008) 28(7):1011–8. doi: 10.1111/j.1478-3231.2008.01733.x
68. Jirova D, Sperlingova I, Halaskova M, Bendova H, Dabrowska L. Immunotoxic effects of carbon tetrachloride—the effect on morphology and function of the immune system in mice. *Cent Eur J Public Health* (1996) 4(1):16–20.
69. Cordoba J, O'Riordan K, Dupuis J, Borensztajn J, Blei AT. Diurnal variation of serum alanine transaminase activity in chronic liver disease. *Hepatology* (1998) 28(6):1724–5. doi: 10.1002/hep.51208640
70. Kim MS, Lee HK, Kim SY, Cho JH. Analysis of the relationship between liver regeneration rate and blood levels. *Pak J Med Sci* (2015) 31(1):31–6. doi: 10.12669/pjms.3115864
71. Schwenger KJ, Clermont-Dejean N, Allard JP. The role of the gut microbiome in chronic liver disease: The clinical evidence revised. *JHEP Rep* (2019) 1(3):214–26. doi: 10.1016/j.jhepr.2019.04.004
72. den Boer M, Voshol PJ, Kuipers F, Havekes LM, Romijn JA. Hepatic steatosis: a mediator of the metabolic syndrome. lessons from animal models. *Arterioscler Thromb Vasc Biol* (2004) 24(4):644–9. doi: 10.1161/01.ATV.0000116217.57583.6e
73. Holm C. Molecular mechanisms regulating hormone-sensitive lipase and lipolysis. *Biochem Soc Trans* (2003) 31(Pt 6):1120–4. doi: 10.1042/bst0311120
74. Voshol PJ, Haemmerle G, Ouwendam DM, Zimmermann R, Zechner R, Teusink B, et al. Increased hepatic insulin sensitivity together with decreased hepatic triglyceride stores in hormone-sensitive lipase-deficient mice. *Endocrinology* (2003) 144(8):3456–62. doi: 10.1210/en.2002-0036
75. Iizuka K, Takao K, Yabe D. ChREBP-mediated regulation of lipid metabolism: Involvement of the gut microbiota, liver, and adipose tissue. *Front Endocrinol (Lausanne)*. (2020) 11:587189. doi: 10.3389/fendo.2020.587189
76. Eberle D, Hegarty B, Bossard P, Ferré P, Foufelle F. SREBP transcription factors: master regulators of lipid homeostasis. *Biochimie* (2004) 86(11):839–48. doi: 10.1016/j.biochi.2004.09.018
77. Lee SD, Tontonoz P. Liver X receptors at the intersection of lipid metabolism and atherosclerosis. *Atherosclerosis* (2015) 242(1):29–36. doi: 10.1016/j.atherosclerosis.2015.06.042
78. Kalhan SC, Edmison J, Marczewski S, Dasarathy S, Gruda LL, Bennett C, et al. Methionine and protein metabolism in non-alcoholic steatohepatitis: evidence for lower rate of transmethylation of methionine. *Clin Sci (Lond)*. (2011) 121(4):179–89. doi: 10.1042/CS20110060
79. Niculescu MD, Zeisel SH. Diet, methyl donors and DNA methylation: interactions between dietary folate, methionine and choline. *J Nutr* (2002) 132(8 Suppl):233S–5S. doi: 10.1093/jn/132.8.233S
80. Elenkov IJ, Wilder RL, Chrousos GP, Vizi ES. The sympathetic nerve—an integrative interface between two supersystems: the brain and the immune system. *Pharmacol Rev* (2000) 52(4):595–638.
81. Bhattacharyya S, Brown DE, Brewer JA, Vogt SK, Muglia LJ. Macrophage glucocorticoid receptors regulate toll-like receptor 4-mediated inflammatory responses by selective inhibition of p38 MAP kinase. *Blood* (2007) 109(10):4313–9. doi: 10.1182/blood-2006-10-048215
82. Izeboud CA, Mocking JA, Monshouwer M, van Miert AS, Witkamp RF. Participation of beta-adrenergic receptors on macrophages in modulation of LPS-induced cytokine release. *J Recept Signal Transduct Res* (1999) 19(1-4):191–202.
83. Krishnan R, Jang YS, Kim JO, Yoon SY, Rajendran R, Oh MJ. Temperature dependent cellular, and epigenetic regulatory mechanisms underlying the antiviral immunity in sevenband grouper to nervous necrosis virus infection. *Fish Shellfish Immunol* (2022) 131:898–907. doi: 10.1016/j.fsi.2022.10.068
84. Walter EJ, Hanna-Jumma S, Carraretto M, Formi L. The pathophysiological basis and consequences of fever. *Crit Care* (2016) 20(1):200. doi: 10.1186/s13054-016-1375-5
85. Lee BH, Inui D, Suh GY, Kim JY, Kwon JY, Park J, et al. Association of body temperature and antipyretic treatments with mortality of critically ill patients with and without sepsis: Multi-centered prospective observational study. *Crit Care* (2012) 16(1):R33. doi: 10.1186/cc11660
86. Young PJ, Saxena M, Beasley R, Bellomo R, Bailey M, Pilcher D, et al. Early peak temperature and mortality in critically ill patients with or without infection. *Intensive Care Med* (2012) 38:437–444. doi: 10.1186/cc10393